FABRICATION OF HETEROEPITAXIAL TEMPLATES FOR GaN-BASED OPTOELECTRONIC DEVICES
Doctoral Dissertation

Teemu Lang

Helsinki University of Technology
Department of Electrical and Communications Engineering
Micro and Nanosciences Laboratory

FABRICATION OF HETEROEPITAXIAL TEMPLATES FOR GaN-BASED OPTOELECTRONIC DEVICES
Doctoral Dissertation

Teemu Lang

Dissertation for the degree of Doctor of Science in Technology to be presented with due permission of the Department of Electrical and Communications Engineering for public examination and debate in Auditorium S4 at Helsinki University of Technology (Espoo, Finland) on the 23rd of February, 2007, at 12 noon.

Helsinki University of Technology
Department of Electrical and Communications Engineering
Micro and Nanosciences Laboratory

Teknillinen korkeakoulu
Sähkö- ja tietoliikennetekniikan osasto
Mikro- ja nanotekniikan laboratorio

HELSINKI UNIVERSITY OF TECHNOLOGY	ABSTRACT OF DOCTORAL DISSERTATION
P. O. BOX 1000, FI-02015 TKK http://www.tkk.fi	

Author	Teemu Lang	

Name of the dissertation

Fabrication of Heteroepitaxial Templates for GaN-based Optoelectronic Devices

Date of manuscript	02.01.2007	Date of the dissertation	23.02.2007
☐ Monograph		☒ Article dissertation (summary + original articles)	

Department	Electronics and Telecommunication
Laboratory	Micro and Nanosciences
Field of research	Electronic materials
Opponent(s)	Prof. Detlef Hommel
Supervisor	Docent Markku Sopanen
(Instructor)	

Abstract

In this work the growth of GaN and AlGaN thin-films by metal-organic chemical vapor deposition (MOCVD) on sapphire substrates is studied. The objective of the study is to improve the performance of optoelectronic devices by reducing the density of threading dislocations (TDs) in nitride semiconductor films. The quality of the thin-films is analyzed by x-ray diffraction (XRD), atomic force microscopy (AFM) and transmission electron microscopy (TEM).

A new multistep method for the growth of a GaN nucleation layer (NL) is presented. The method consists of cyclically depositing a layer of GaN at a lower temperature (LT-GaN) and recrystallizing this layer into GaN islands in an *in-situ* annealing step. After the recrystallization a new LT-GaN layer can be deposited and recrystallized onto the existing islands to increase their size. The method enables a reduction in the density of nucleation islands (NIs) and their boundaries. AFM is utilized to demonstrate a reduction in the density NIs to a value of 1.7×10^7 cm^{-2}.

Process parameter optimization is utilized to stimulate growth of NIs in the vertical direction. This causes TDs to incline inside the NIs, which is demonstrated by TEM. A smaller density for the NIs enables a prolonged vertical growth period enhancing the inclination of TDs. Theoretical studies indicate that inclined TDs are able to react with each other by annihilation or fusion. The multistep method is used to fabricate GaN thin-films with a TD density of only 5×10^7 cm^{-2}. This result is demonstrated by AFM and TEM measurements. Qualitatively the improvement in crystalline quality is demonstrated by XRD.

Finally the multistep method is adapted to the MOCVD growth of $Al_{0.12}Ga_{0.88}N$ layers on sapphire substrates. The method is used to grow crack-free $Al_{0.12}Ga_{0.88}N$ layers with a thickness of 2 μm on a GaN NL. A TD density of 5×10^8 cm^{-2} in these films is demonstrated by AFM and XRD. TEM is used to study the relaxation of the films and the formation of TDs at the $Al_{0.12}Ga_{0.88}N$-substrate interface.

Keywords	MOCVD, GaN, AlGaN, threading dislocation	
ISBN (printed)	978-951-22-8611-9	ISSN (printed)	1795-2239
ISBN (pdf)	978-951-22-8612-6	ISSN (pdf)	1795-4584
ISBN (others)		Number of pages	54 p. + app. 56 p.
Publisher	TKK		
Print distribution	TKK, Micro and Nanosciences Laboratory		
☒ The dissertation can be read at http://lib.tkk.fi/Diss/2007/isbn9789512286126/			

Tekijä   Teemu Lang

Väitöskirjan nimi

Heteroepitaksiaalisten alustakiteiden valmistus GaN-pohjaisiin optoelektronisiin komponentteihin

Tiivistelmä

Tässä työssä tutkitaan GaN ja AlGaN ohutkalvojen valmistusta safiirialustalle metallo-orgaanisella kaasufaasikasvatuksella (MOCVD). Tavoitteena on etenevien dislokaatioiden tiheyden pienentäminen nitridipuolijohdekalvoissa optoelektronisten komponenttien suorituskyvyn parantamiseksi. Ohutkalvojen laatua analysoidaan röntgendiffraktiolla (XRD), atomivoimamikroskopialla (AFM) ja transmissioelektronimikroskopialla (TEM).

Työssä esitetään uusi monivaiheinen menetelmä GaN ydintymiskerroksen valmistamiseksi. Menetelmässä valmistetaan jaksoittain ensin matalammassa lämpötilassa järjestäytymätön GaN kerros, joka kiteytetään GaN saarekkeiksi *in-situ* lämpökäsittelyllä. Kiteyttämisen jälkeen saarekkeiden päälle valmistetaan uusi matalamman lämpötilan GaN kerros, joka voidaan jälleen kiteyttää saarekekoon kasvattamiseksi. Menetelmä mahdollistaa ydintymissaarekkeiden sekä näiden välisten rajapintojen tiheyden pienentämisen. AFM mittauksilla osoitetaan ydintymissaarekkeiden tiheyden pieneneminen arvoon $1{,}7\times10^7$ cm^{-2}.

Prosessiparametrien optimoinnilla ydintymissaarekkeet saadaan kasvamaan pystysuunnassa, mikä aiheuttaa etenevien dislokaatioiden taipumista ydintymissaarekkeiden sisällä. Tämä osoitetaan TEM mittauksilla. Pienempi saareketiheys GaN ydintymiskerroksessa mahdollistaa pidemmän ajan ydintymissaarekkeiden pystysuuntaiselle kasvulle, mikä on edullista etenevien dislokaatioiden taipumiselle. Teoreettinen tarkastelu osoittaa, että taipuneet etenevät dislokaatiot voivat kohdatessaan reagoida toistensa kanssa annihiloitumalla tai fuusioitumalla. Monivaiheisella menetelmällä valmistetaan heteroepitaksiaalisia GaN ohutkalvoja, joissa etenevien dislokaatioiden tiheys on vain 5×10^7 cm^{-2}. Tämä tulos osoitetaan AFM ja TEM mittauksilla. Kvalitatiivisesti kidelaadun paraneminen osoitetaan XRD mittauksilla.

Lopulta monivaiheista valmistusmenetelmää sovelletaan $Al_{0.12}Ga_{0.88}N$ kalvojen MOCVD valmistukseen safiirisubstraatille. Menetelmällä valmistetaan n. 2 µm paksuisia halkeilemattomia $Al_{0.12}Ga_{0.88}N$ kalvoja GaN ydintymiskerroksen päälle. Kalvoissa etenevien dislokaatioiden tiheys on 5×10^8 cm^{-2}. Tämä tulos osoitetaan AFM ja XRD mittauksilla. TEM mittauksilla selvitetään kalvojen relaksoitumista sekä etenevien dislokaatioiden muodostumista $Al_{0.12}Ga_{0.88}N$-substraatti rajapintaan.

Preface

The work presented in this thesis has been carried out at the Optoelectronics Laboratory of Helsinki University of Technology during 2004-2006.

I want to express my gratitude to Professor Harri Lipsanen and to Docent Markku Sopanen, the supervisor of this thesis, for their guidance throughout the period of my work. Professor Lipsanen initiated the research of nitride semiconductors at the Optoelectronics Laboratory giving me the opportunity to work in a very interesting field of science. I want to especially thank Dr. Maxim Odnoblyudov and Dr. Vladislav Bougrov from Abraham-Ioffe Institute and OptoGaN Oy for their invaluable support and ideas concerning my research. Thank you for the many fruitful discussions. Furthermore I want to thank the personnel of the laboratory and especially my colleagues in the nitrides research team, Mr. Sami Suihkonen, Mr. Olli Svensk and Mr. Pekka Törmä. Thank you for the enlightening discussions and the fun times in the lab.

The Graduate School of Electronics and Telecommunication and OptoGaN Oy are acknowledged for the financial support of this work.

Finally I want to thank my girlfriend Pia for her support and patience, and my brother and my parents for their encouragement.

Espoo, 2nd January 2007   Teemu Lang

Contents

List of publications

This thesis consists of an overview and of the following publications that are referred to in the text by their Roman numerals.

I.   V. E. Bougrov, M. A. Odnoblyudov, A. E. Romanov, T. Lang, O. V. Konstantinov, Threading dislocation density reduction in two-stage growth of GaN layers, physica status solidi (a) 203 (2006) R25.

II.   T. Lang, M. A. Odnoblyudov, V. E. Bougrov, M. Sopanen, MOCVD growth of GaN islands by multistep nucleation layer technique, Journal of Crystal Growth 277 (2005) 64.

III.   T. Lang, M. A. Odnoblyudov, V. E. Bougrov, S. Suihkonen, M. Sopanen, H. Lipsanen, Morphology optimization of MOCVD-grown GaN nucleation layers by the multistep technique, Journal of Crystal Growth 292 (2006) 26.

IV.   T. Lang, M. A. Odnoblyudov, V. E. Bougrov, A. E. Romanov, S. Suihkonen, M. Sopanen, H. Lipsanen, Multistep method for threading dislocation density reduction in MOCVD grown GaN epilayers, physica status solidi (a) 203 (2006) R76.

V.   T. Lang, M. A. Odnoblyudov, V. E. Bougrov, S. Suihkonen, O. Svensk, P. T. Törmä, M. Sopanen, H. Lipsanen, Reduction of threading dislocation density in $Al_{0.12}Ga_{0.88}N$ epilayers by a multistep technique, Journal of Crystal Growth (2007), IN PRESS.

VI.   S. Suihkonen, O. Svensk, T. Lang, H. Lipsanen, M. A. Odnoblyudov, V. E. Bougrov, The effect of InGaN/GaN MQW hydrogen treatment and threading dislocation optimization on GaN LED efficiency, Journal of Crystal Growth (2007), IN PRESS.

VII.   O. Svensk, S. Suihkonen, T. Lang, H. Lipsanen, M. Sopanen, M. A. Odnoblyudov, V. E. Bougrov, Effect of growth conditions on electrical properties of Mg-doped p-GaN, Journal of Crystal Growth (2007), IN PRESS.

Author's contribution

The author has written the manuscripts and designed the experiments for publications II, III, IV and V.

The author has performed the major part of the data collection, data analysis and sample fabrication for publications II, III, IV and V.

The author has performed parts of the sample fabrication and data collection for publications VI and VII. The author has significantly contributed to the device processing for publication VI and in the post-growth processing of samples for publication VII.

The author has contributed to the design of experiments, performed parts of the sample fabrication and assisted in writing of the manuscript for publication I.

1 Introduction

The blue light emitting diode (LED) and the blue laser diode (LD) are currently finding their way into consumer applications such as full-colour LED displays and DVD players. The shorter wavelength of blue light enables more efficient data storage and readout in the next generation DVD standards. LEDs are also gradually being applied into general lighting such as flashlights, indoor lighting, flat-panel backlighting and traffic signalling. In cases where white light is needed blue and ultra-violet (UV) LEDs can be used as pump sources to excite broadband phosphors. These phosphors acting as wavelength converters emit light with a spectrum complementing the LED emission spectrum for white light generation.

To date there exist few semiconductor material systems that have been studied for efficient blue-light emission. SiC- and ZnSe-based devices initially showed more promise over GaN-based structures. During the last couple of decades, however, significant progress has been made in the area of epitaxial growth of group III nitride semiconductors. Specifically GaN and ternaries InGaN and AlGaN have been studied intensively since these are the compounds required for blue and UV light emitting structures. Among the key inventions leading to the development of a blue GaN-based LED was the growth process including a low temperature (LT) nucleation layer (NL) [1] for reduced threading dislocation density in GaN epilayers. Mg-doped GaN [2] with p-type conductivity sufficient for high power LEDs and LDs was developed by S. Nakamura and co-workers [3] in 1991. Additionally, significant progress in the contacting technology for GaN [4] has contributed to the advances towards more efficient solid-state blue light emitters. Currently the III-nitrides are considered as the best material system for efficient solid-state general lighting applications.

The problems related to the operation of high power GaN-based light emitting devices mainly concern the crystal quality of heteroepitaxial films, p-type doping and p-type contacting technology. The objective of this doctoral work is to address the issue of crystal quality by reducing the density of threading dislocations (TDs) in the III-nitride structures. To this end new metalorganic chemical vapor deposition (MOCVD) techniques were developed for the growth of GaN and AlGaN films.

In chapter two of this dissertation the material properties of GaN are reviewed. Chapter three presents the methods and equipment used for the characterization of the GaN films grown for our studies. Chapter four describes the epitaxial growth of GaN including a

discussion about the most common substrate materials, precursors and a review of the widely used two-step growth method. In this context a generally accepted model for MOCVD growth of GaN on c-plane sapphire is considered. Chapters two and four rely mainly on previously reported results in GaN research. These chapters lay the background for our own studies and results, which are discussed in chapters five through seven. Chapter five concentrates on the reduction of the TD density (TDD) from a theoretical perspective and the mechanisms behind TDD reduction are reviewed. In this chapter a new approach for TDD reduction is discussed. Chapter six describes the experimental work carried out to develop the new multistep MOCVD growth method for GaN films with a reduced TDD. In the beginning of this chapter the growth of GaN nucleation islands is discussed. The latter part of the chapter focuses on the overgrowth of these islands to eventually obtain a smooth film with a reduced TDD. Chapter seven discusses how the developed method for the growth of high quality GaN is adopted for AlGaN growth.

2. Fundamentals of GaN

This chapter provides a short review of the most important properties of GaN for optoelectronic applications. These properties include the crystal structure of the group III nitrides and the electronic band structure of GaN. The most useful ternary compounds in the III-nitride system, InGaN and AlGaN, are briefly reviewed. These ternaries find applications in most III-nitride based LED structures. Other GaN material properties relevant from the applications point of view are also discussed. The important topic of dislocations in GaN is discussed in the context of epitaxial growth in chapter 4.

2.1 Crystal structure

GaN and its related compounds AlN and InN can crystallize either in a cubic zinc blende or in a hexagonal wurtzite structure. Both of these phases can be grown by different thin film methods and they have been extensively studied since the invention of the blue GaN LED. Commercial optoelectronic devices are most commonly based on the wurtzite structure due to its superior thermal stability at high operating temperatures. Additionally, the electrical properties of the two different crystal structures have significant differences. This work concentrates exclusively on the wurtzite GaN and AlGaN.

Atoms in both the zinc blende and the wurtzite lattice are tetrahedrally bonded to the nearest neighbors. The two crystal structures differ in their stacking sequence and Bravais lattice. Fig. 2.1 shows the clinographic projection of a wurtzite GaN unit cell consisting of lattice planes with only one element, either N or Ga. In one lattice plane the relative positioning of atoms is such that they form hexagons. The in-plane lattice constants in Fig. 2.1 are labeled a and b. Lattice constant c signifies the spacing of two identical lattice planes. Values for these constants are given in Table 1 [5] along with the lattice constants for sapphire, the most commonly used substrate material for wurtzite GaN. The crystal growth of GaN on sapphire is challenging due to the large in-plane lattice mismatch between the two compounds. When grown on a (0001) sapphire surface the wurtzite GaN crystal is rotated 30° relative to the underlying substrate to minimize stress. This results in a 16% lattice mismatch ($\Delta a_{epi}/\Delta a_{sub}$) in the basal plane as illustrated in Fig. 2.2.
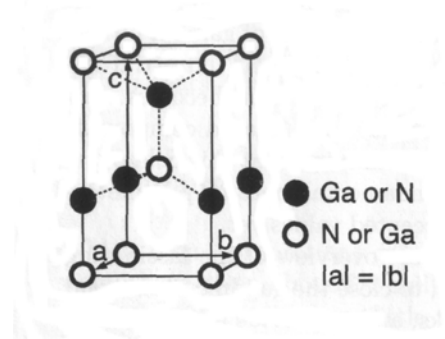
Figure 2.1. Unit cell of wurtzite GaN.

Table 1. Lattice constants for sapphire and hexagonal (wurtzite) GaN.

Lattice constant (Å)	A	C
Sapphire	4.758	12.991
GaN	3.186	5.182
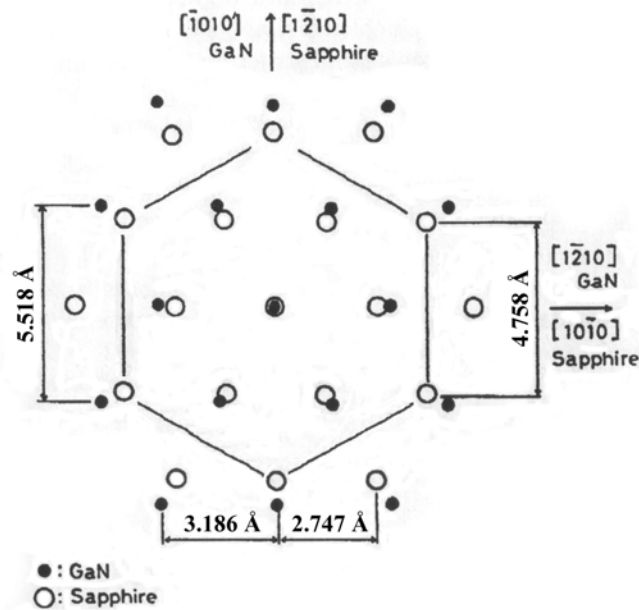
Figure 2.2. The epitaxial relationship of wurtzite GaN and c-plane sapphire.

The structure of the wurtzite unit cell results in an internal asymmetry along the c-axis. Therefore, the directions of the bonds between atoms are different along [0001] and

[000$\bar{1}$] resulting in an internal polarity of the film. This polarity is defined by the direction of the group III–N bond, which is aligned parallel to the c-axis. Depending on the relative placement of the group III and N atoms the GaN film is called either Ga- or N-polar. Polarity effects in GaN and its alloys are an important field of study [6,7]. These issues have implications all the way up to the device level. GaN obtained by MOCVD processes on c-plane sapphire is commonly Ga-polar. The unit cell structure for the two polarities is illustrated in Fig. 2.3.
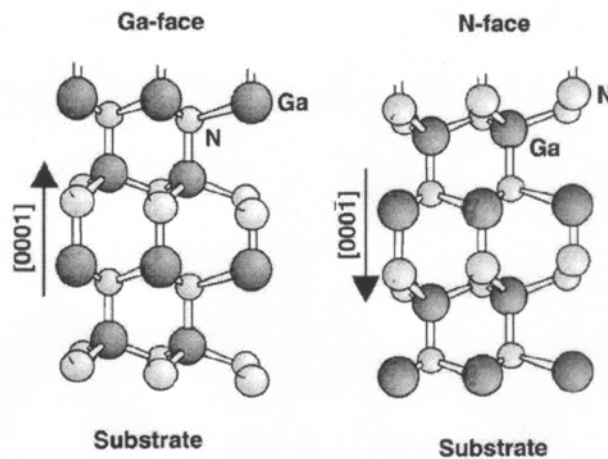
Figure 2.3. Crystal structure of the Ga- and N-polar GaN [8].

2.2 Electronic band structure

The III-nitride semiconductors are direct band-gap materials. This is a necessity for efficient light generation inside the materials. Band structure studies for GaN [9], AlN [10], InN [11] and $Al_xGa_{1-x}N$ [12] can be found in the literature.

The electronic band structures of wurtzite GaN and its cubic zinc blende counterpart are very similar. The biggest difference is the non-parabolicity of valence bands in wurtzite GaN. As a result the theoretical studies about the band structure in hexagonal and cubic GaN are somewhat different as the effective mass approximation fails for the wurtzite structure. From the applications point of view the key difference between the band structures of the two crystalline phases is the larger bandgap of wurtzite GaN. Additionally, in the wurtzite structure quantum well confinement and strain effects on the energy bands are much less pronounced than in cubic semiconductors. Fig. 2.4 illustrates the calculated energy band structure for wurtzite GaN near the fundamental gap at k=0 in

5

the k-space [13]. The valence band maximum (VBM) and the conduction band minimum (CBM) have the same k-value necessary for efficient radiative recombination to take place. The top of the valence band is split into three different bands (the A, B and C bands) by the crystal field (band C) and by the spin-orbit coupling (band B). These bands and their corresponding exciton energies in the bandgap are labeled in Fig. 2.4. The temperature dependence of the interband transitions in wurtzite GaN has been studied in Ref. 14.
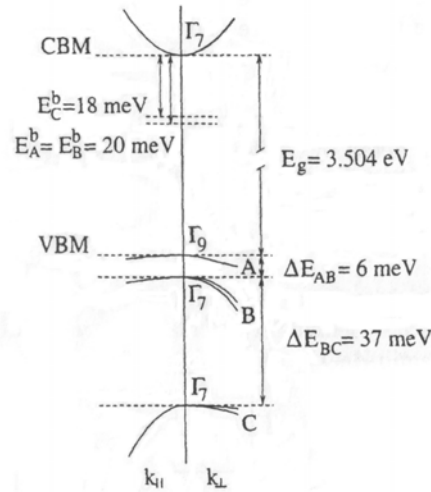
Figure 2.4. Electronic band structure of hexagonal GaN [13].

The ternaries InGaN and AlGaN together with GaN are the most common group III nitride semiconductors encountered in commercial applications. In and Al are incorporated into the GaN lattice to decrease and increase the bandgap of the crystal, respectively. Fig. 2.5 illustrates the bandgap as a function of the a-axis lattice constant in the III-nitride system. As can be observed from the figure the bandgap energies in the III-nitride system cover the entire visible spectrum continuing all the way up to the deep ultraviolet region. As the In and Al content increases in InGaN and AlGaN films, respectively, the growth of high quality crystals becomes more difficult. This currently limits the operational wavelength region of GaN-based light-emitters from green to near UV. The fabrication on GaN-based devices emitting in the red and deep UV wavelength regions remains challenging.
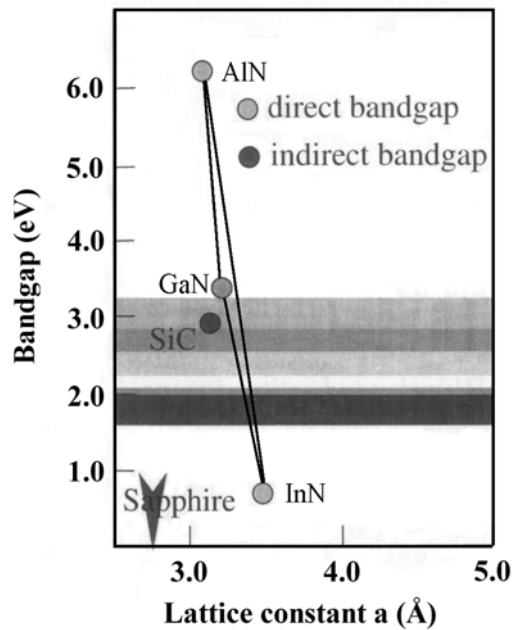
Figure 2.5. The energy bandgap of III-nitride binary compounds vs. their lattice constant a.

2.3 Material properties

The group III nitrides possess some exceptional features, which have a profound impact on the device design from these materials. GaN and its related compounds are extremely hard materials. This mechanical stability combined with chemical inertness makes the processing of GaN-based devices very challenging [15]. Thus far no chemical wet-etching process has been discovered to pattern these materials with the required accuracy needed for device fabrication. The only possibility is to combine physical and chemical etching in a plasma process. The most commonly used dry etching techniques are reactive ion etching (RIE) and chemically assisted ion beam etching (CAIBE). In thicker structures such as lasers where a faster etching rate and vertical sidewall profiles are essential chlorine-based inductive coupled plasma etching (ICP-RIE) processes are often utilized [4].

Even though the stability of group III nitrides presents some technological challenges to device fabrication these material properties are also the very reason that make GaN-based material systems attractive for commercial applications. Specifically good thermal stability and conductivity are of importance in power applications such as high electron mobility transistors (HEMTs) for power amplifiers in X-band radars and high brightness LEDs. In practice, heat extraction from GaN-based devices still remains an issue due to the low thermal conductivity of sapphire substrates.

7

As briefly discussed in section 2.1 the wurtzite crystal of the group III nitrides is polarized and exhibits piezoelectric fields in the material. The origin of this spontaneous polarization lies in the strong ionic nature of the Ga-N bond [16]. When the III-nitride crystal is deformed due to external forces such as compressive or tensile stress a piezoelectric polarization is induced to the crystal. The total polarization in the crystal is the sum of the spontaneous and the piezoelectric components.

An example of a detrimental effect caused by piezoelectric fields in a crystal is the displacement of the electron and hole wavefunction in an InGaN/GaN quantum well structure (Fig. 2.6). This effect reduces the overlapping of the electron and hole wavefunctions decreasing the internal quantum efficiency of the structure [17]. Additionally the energy difference between the electron and hole states decreases causing a red shift in the emission spectrum of the structure. This phenomenon is known as the quantum confined Stark effect (QCSE) [18].

Thus far piezoelectric effects have not been of major concern in optoelectronic devices due to the high current densities at which these components are commonly operated. Only recently has this issue gained more attention due to the quest towards improved internal quantum efficiency in light-emitting devices [19] targeted for general lighting applications.
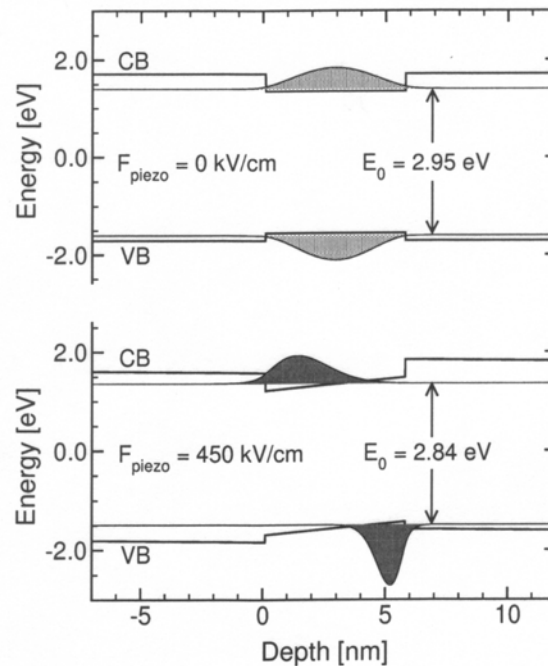
Figure 2.6. Schematic illustration of the effect of a piezoelectric field on the carrier wavefunctions in a quantum well [20].

3. Characterization methods

This chapter presents the procedures and the equipment used in this thesis for the characterization of thin-films. A review of the determination of TDD by x-ray diffraction (XRD) is presented along with an outline of the XRD system. Furthermore, the AFM equipment used for this work is presented along with the etch-pit density (EPD) measurement procedure. The fundamentals of *in-situ* reflectometry in thin-film characterization are also reviewed.

3.1 *In-situ* reflectometry

The measurement setup for *in-situ* reflectometry in the MOCVD system used for this work is illustrated in Fig. 3.1. The setup operates in normal incidence geometry. A broadband source emits light through a beam splitter and an optical probe on to the rotating susceptor. Part of the incident beam is reflected back to the beam splitter from the surface of the susceptor. This reflected signal is deflected by the beam splitter and guided in an optical fiber through a bandpass filter. The filter selects a narrow measurement band from the wideband signal. The measurement wavelength of the reflectometer used in this thesis was 638 nm. The reflectivity of the surface of the growing thin film can be accurately monitored *in-situ* as the samples pass under the broadband beam incident on the susceptor. The intensity of the reflected signal at the selected wavelength is measured by a photodetector. To identify different samples and positions on the susceptor from the resulting reflectivity curve a rotation signal is also fed into the measurement computer for reference.

In an alternative setup the broadband light source can be replaced by a laser operating at the desired measurement wavelength. In this case the bandpass filter, which selects the narrow measurement band, is no longer required. This setup with a laser (operating at a wavelength of 638 nm) as the light source was used in the work for publications II and III.

In a single-layer structure illustrated schematically in Fig. 3.2 the surface reflectance for normal incidence at wavelength λ can be expressed as

$$R_0 = \frac{r_{12}^2 + 2r_{12}r_{23}\cos(2\alpha) + r_{23}^2}{1 + 2r_{12}r_{23}\cos(2\alpha) + r_{12}^2 r_{23}^2}, \alpha = \frac{2\pi N_2 d}{\lambda},$$ (3.1)

where r_{ij} and t_{ij} are the reflectivity coefficient and the transmission coefficient, respectively, at the interface between materials i and j. N_2 and d are the refractive index and the thickness of the growing film. Eq. 3.1 takes into account the interference of light reflected from the two boundaries between materials 1 and 2 (air-film) and between materials 2 and 3 (film-substrate). The equation applies for non-absorbing materials with smooth surfaces. The growth rate of a film can be calculated from the oscillation period of the measured *in-situ* reflectance data using Eq. 3.1. Since the oscillation period of a growing film is 2α it can be shown that the growth rate is given by

$$GR = \frac{\lambda}{2N_2 \tau},$$ (3.2)

where τ is the oscillation period.
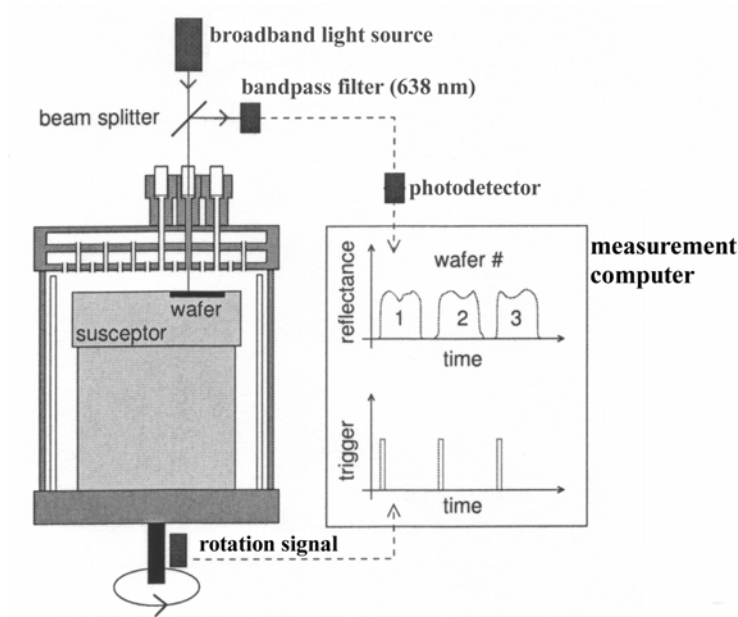
Figure 3.1. The measurement setup for *in-situ* reflectometry in the MOCVD system used for this work.
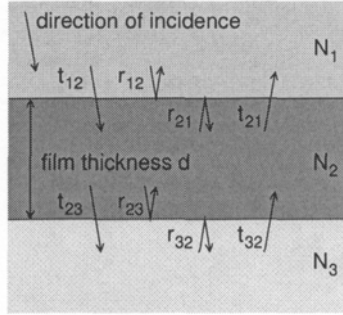
Figure 3.2. Notations used for the derivation of reflectance in a one-film structure.

When the film surface is not perfectly smooth but exhibits notable roughness compared to the measurement wavelength the reflectance value given by Eq. 3.1 does not adequately correspond to the measured value. The effect of surface roughness can be taken into account by a model based on a Gaussian distribution of heights about the mean value [21]. In this case the surface reflectance is given by

$$R = R_0 \exp[-(4\pi\sigma)^2 / \lambda^2],$$ (3.3)

where σ is the root-mean-square (RMS) surface roughness.

In GaN processes the surface reflectance is determined by the interplay between interference effects and surface roughness. This will be discussed in section 4.3.

3.2 Atomic force microscopy

Atomic force microscopy (AFM) was used in this work mainly to measure the etch-pit density (EPD) of AlGaN and GaN buffer layers and the surface morphology of GaN nucleation layers (NLs). For these purposes the method is extremely practical since it requires very little sample preparation and the measurements can be carried out at room temperature.

The operating principle of the AFM system used for this work is illustrated in Fig. 3.3. A laser beam is focused on the tip of a silicon nitride (SiN) cantilever probe. The beam is reflected from the tip to a segmented photodetector. The inspected sample is mounted on a moving sample holder, which can be displaced laterally by piezoelectric actuators. The sample moves under the cantilever probe, which responds to the height variations on the surface of the sample through Coulomb or van der Waals interactions. This results in vertical displacement of the cantilever and the reflected laser spot on the photodetector. A correction signal is fed back from the photodetector to a vertical piezoelectric actuator.

11

This actuator adjusts the vertical position of the sample to keep the cantilever probe at a constant height, *i.e.*, to keep the reflected laser beam spot at a constant point on the photodetector. This way the correction signal reflects the surface morphology of the sample.

The GaN films in this thesis were characterized by a Nanoscope IIIE atomic force microscope. Its vertical resolution is 0.1 nm and the maximum scan area is 13 μm x 13 μm. The vertical resolution is sufficient for distinguishing individual atomic steps on the sample surface. The lateral resolution depends on the particular surface morphology of the scanned sample. It is typically in the range of ten nanometers. The smallest lateral features of interest on the studied III-nitride films for this work were etch pits on an $Al_{0.12}Ga_{0.88}N$ film. These features had lateral dimensions in the order of 100 nm.
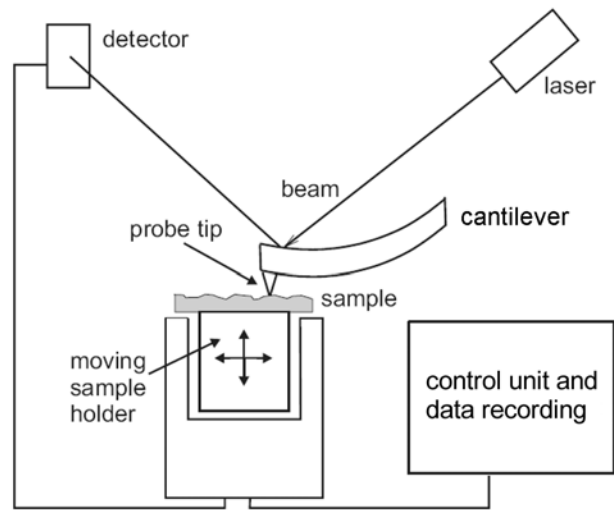
Figure 3.3. Operating principle of the AFM apparatus used in this work.

3.2.1 Etch-pit density measurements

The primary method to quantitatively evaluate the TDD in this work was to characterize the surface morphology of a wet etched III-nitride film by AFM. These etch-pit density (EPD) measurements have evolved to a widely used characterization method for the determination of TDD. The TDD values obtained from EPD measurements are known to correlate well with the results obtained by other characterization methods such as transmission electron microscopy (TEM) [22]. Furthermore, EPD measurements are easy to implement as they only involve short pre-treatment of the samples in an acid solution prior to a regular AFM or a scanning electron microscope (SEM) measurement.

Several etchants have been studied for EPD measurements of III-nitride layers [22, 23]. The chemicals in the sample preparation for EPD measurements are chosen so that the points where threading dislocations are terminated on the surface of the film are

selectively etched. This requires that the etchant is capable of crystallographic selectivity [24]. In this work a 1:1 mixture of hot (240 °C) sulphuric and phosphoric acids was used to etch the surface of GaN and AlGaN films prior to the AFM measurement.

3.3 X-ray diffraction

X-ray diffraction (XRD) was used in this work for qualitative comparison of the TD densities between different samples and to support the results obtained from EPD measurements. A schematic of the high-resolution x-ray diffraction (HR-XRD) system used in this work is illustrated in Fig. 3.4. The system is a Philips X'Pert Pro diffractometer, which was operated in a triple axis configuration. In this setup an analyzer crystal is placed in front of the detector in the diffracted beam path to improve angular resolution. The incident beam monochromator is a four-crystal Ge monochromator tuned to select the Cu-$K\alpha_1$ peak from the emission spectrum of the x-ray tube. In front of the monochromator an x-ray mirror was utilized in order to reduce the divergence of the incident beam.
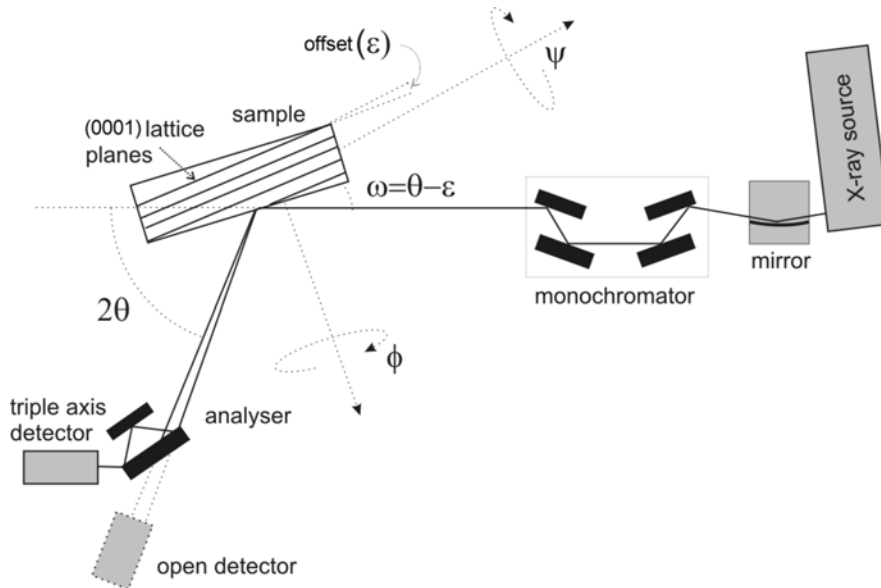
Figure 3.4. Schematic of the XRD measurement setup. This setup was utilized to perform the high resolution (HR) XRD scans on the studied III-nitride films.

A GaN or AlGaN crystal can be roughly described by means of a mosaic model [20]. In this model the nitride film is composed of hexagonal grains. The individual grains exhibit in-plane twist and out-of-plane tilt with respect to each other. These distortions result in

threading dislocations in the crystal as will be discussed in section 4.4. In the framework of the mosaic crystal model film coherence can be thought of as the average size of the grains. The finite film coherence and the threading defects in the crystal result in broadening of the x-ray diffraction peaks.

Threading dislocations having a Burgers vector parallel to the film-substrate interface do not distort the <001> crystal planes. In order to characterize the threading dislocation content in a III-nitride film the distortion of asymmetric crystal planes has to be measured [25]. To this end the peak widths of the (302) asymmetric diffraction were measured to take into account the effect of all types of threading dislocations.

4. Epitaxial growth of GaN

In this chapter the growth of high-quality GaN on c-plane sapphire is discussed. The focus will be exclusively on metalorganic chemical vapor deposition (MOCVD). Main features of the MOCVD system used for the growth of the samples studied in this work are outlined. Fundamentals of various MOCVD growth processes for group III nitrides are also discussed. The widely used two-step growth method for GaN is discussed in more detail and in this context a generally accepted growth model for GaN is presented. Furthermore, the chapter reviews the current state of substrate development for GaN epitaxy. The generation of dislocations in the growth of GaN on c-plane sapphire is described in section 4.4 followed by a discussion about current methods to reduce the TD density.

4.1 Substrate materials

The work on group III nitrides is based on heteroepitaxy since the availability of GaN single crystal substrates is poor and their price is extremely high. GaN can be grown on substrates like silicon (111), SiC, zinc oxide and sapphire. SiC exists in many polytypes of which 4H and 6H are most commonly used for GaN growth. The benefits of a SiC substrate are good thermal conductivity and a smaller lattice mismatch to GaN when compared to those of sapphire, the most widely used substrate for optoelectronic applications. A drawback of SiC as a substrate material is its smaller thermal expansion coefficient with respect to GaN. This leads to tensile stresses in the GaN layer as thin film structures are cooled down from the growth temperature to room temperature. Furthermore, the difficulty in the fabrication of SiC of a particular polytype makes these substrates fairly expensive.

By far the most popular substrate for optoelectronic applications is sapphire with a (0001) oriented surface, which has the benefit of very good thermal stability. Additionally, sapphire substrates are inexpensive making them very suitable for volume production. C-plane (0001) sapphire was the substrate material of choice for every growth experiment in this work.

As mentioned in section 2.1 GaN exhibits a 16% lattice mismatch on c-plane sapphire. This is clearly too much for highly coherent crystal growth as it results in a critical thickness of only a few nanometers [26]. Another downside of using sapphire as a substrate material for GaN is the difference in their thermal expansion coefficients. The in-plane thermal expansion coefficients for GaN and sapphire are $5x10^{-6}$ K^{-1} and $8x10^{-6}$ K^{-1}, respectively [27]. This leads to compressive strain in GaN films at room temperature.

4.2 Metalorganic chemical vapor deposition

Since the 1960's MOCVD, also known as metalorganic vapor phase epitaxy (MOVPE), has evolved into a widely used method for the fabrication of semiconductor thin films. The technology is used in research as well as in volume production of semiconductor device structures. MOCVD uses metalorganic precursors that thermally decompose in the gas phase and react on a heated substrate. MOCVD can be used to fabricate structures where smooth and abrupt interfaces between epitaxial thin films of different composition are required. Furthermore, the technique allows for accurate control of composition, doping and thickness of the layer virtually over the entire substrate wafer.

Rapid development of the group III nitride technology during the recent years has significantly increased the industrial use of MOCVD. Particularly the commercialization of white and blue LEDs and blue lasers [28,29,30] has had a profound impact on the sales of MOCVD systems. A popular alternative technology for MOCVD is molecular beam epitaxy (MBE). Although used in research for GaN-based materials the commercial application of MBE is primarily dedicated for the fabrication of conventional III-V compound semiconductors and their heterostructures.

The MOCVD system used for the research reported in this work was a vertical flow close coupled showerhead (CCS) reactor manufactured by Thomas Swan Scientific Equipment. The system was installed at the Optoelectronics Laboratory in the Micronova research center of the Helsinki University of Technology in 2002. A schematic gas-flow diagram of the apparatus is illustrated in Fig. 4.1. The metalorganic precursors are located in bubbler sources submerged in temperature-controlled fluid. In this way the vapor pressure of each precursor can be accurately regulated. Gaseous precursors are guided into the reaction chamber in carrier gas through a network of computer-controlled mass-flow controllers and valves. The nonmetal precursors arrive into the reaction chamber through a separate pipework in order to reduce the possibility of pre-reactions between the reagents. A more detailed schematic of the reaction chamber can be found in Fig. 4.2. The reaction chamber of the system can fit three 2" wafers on a SiC-coated graphite susceptor. The susceptor rotates during operation to produce a more homogeneous flux of precursor molecules on the substrates. The susceptor is resistively heated from underneath by a tungsten coil to produce substrate temperatures of up to 1500 °C. The desired pressure is maintained in the reaction chamber by a computer-controlled valve connected to a dry pump.
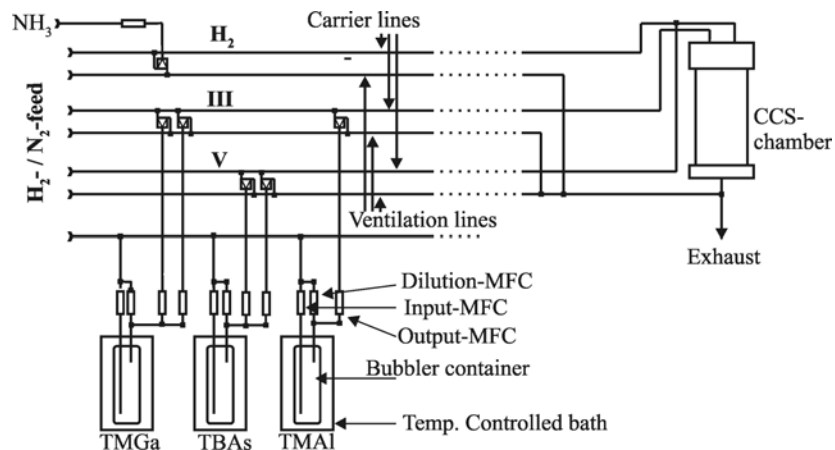
Figure 4.1. Gas-flow diagram for the CCS MOCVD reactor used in this work.
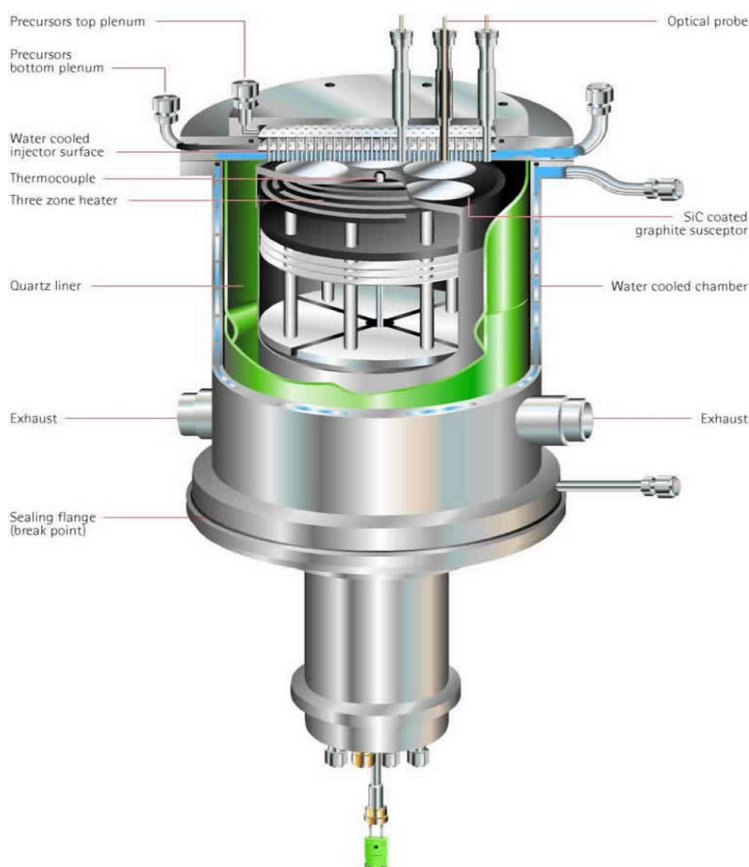
Figure 4.2. Structure of the CCS reaction chamber in the MOCVD system.

The crystal growth processes in MOCVD are based on chemical reactions on and above the heated substrates. The common source materials involved in the synthesis of GaN are

ammonia (NH$_3$) and trimethylgallium (TMGa or Ga(CH$_3$)$_3$) and the carrier gas is either nitrogen (N$_2$) or hydrogen (H$_2$). Various chemical reactions are involved in the GaN growth process [31]. The most important ones are the thermal decomposition reactions as a result of which Ga and N atoms become available for nucleation on the surface of the growing thin film. The CCS reactor design prevents ammonia molecules from decomposing until they reach a distance of about one centimeter from the susceptor. This keeps the molar fraction of decomposed ammonia negligible in the reactor. Therefore, in the system used for this work, the reaction governing the growth of the GaN crystal is

$$Ga(g) + NH_3(g) \Leftrightarrow GaN(s) + \frac{3}{2}H_2(g). \tag{4.1}$$
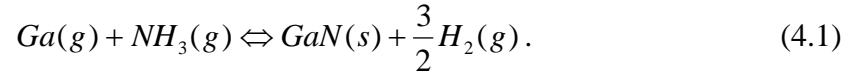
This reaction is valid for the commonly used temperature range of about 600-1100°C in the MOCVD growth of GaN. As Eq. 4.1 is reversible the introduction of excess hydrogen will result in the reverse reaction and decomposition of GaN. As will be discussed later this property of the GaN MOCVD process can be exploited in the reduction of the TDD of GaN films.

The rate at which the forward and backward reactions in Eq. 4.1 occur is dictated by the partial pressure of each reagent in the surrounding atmosphere. In a closed environment the reaction would gradually reach an equilibrium point at which the forward and backward reactions occur at the same rate. In this case neither net film growth nor decomposition can occur. The position of this equilibrium is dictated by thermodynamics, mainly temperature and total pressure. In order to keep the rate of the forward reaction faster than the rate of the backward reaction, *i.e.,* in order to achieve film growth, a continuous flow of gallium and nitrogen has to be supplied into the reaction chamber. Simultaneously the reaction byproducts such as hydrogen have to be removed from the chamber to maintain a steady growth rate.

4.3 The two-step method

Initially the growth of GaN was attempted directly on nitridated sapphire [32]. This growth technique resulted in polycrystalline film with a rough surface. The TD density of these types of films was extremely high (in the order of 10^{10}-10^{11} cm^{-2}). In the late 1980's a two-step growth method for GaN was developed [1]. The method employed an AlN layer in between the sapphire substrate and the GaN layer. The 50-100 nm thick AlN NL was grown at a lower temperature (LT) than the overgrown GaN layer. The new method resulted in a significant reduction of the TDD and in smooth specular GaN films. The two-step method can be considered as one of the key inventions resulting in the commercialization of GaN-based light-emitting devices.

In addition to AlN, LT GaN is also a suitable material for the NL [5]. Fig. 4.3 shows a schematic illustration of a widely used two-step growth process for GaN employing a LT

GaN NL. A hydrogen carrier-gas flow is present throughout the process. The sapphire substrate is initially annealed in hydrogen ambient at about 1080 °C for the removal of possible impurities. Temperature is subsequently decreased to about 800 °C at which point the ammonia flow is switched on. This nitridates the substrate forming a thin layer of AlN on the surface. Next, temperature is further decreased to about 530 °C. This is the point where the TMGa flow is switched on and the growth of a LT GaN NL begins. LT growth is continued until the GaN layer reaches a thickness of 40-100 nm. Subsequently, temperature is increased back to a higher value after which GaN growth is initiated again. The growth of this high-temperature (HT) GaN continues until the desired thickness is reached.
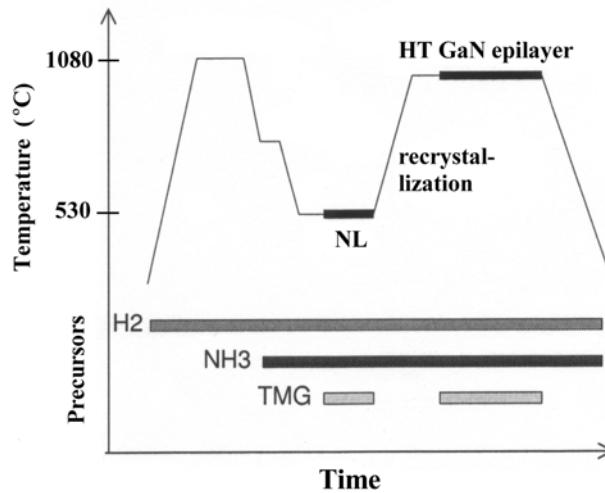
Figure 4.3. Diagram illustrating the temperature profile and the timing of precursor flows during the two-step growth of GaN.

The widely accepted growth model for GaN in the two-step process is illustrated schematically in Fig. 4.4. The graph in the figure presents how the reflectivity of the surface of the sample changes throughout a conventional two-step process. Critical points in the process are labeled in the graph. Reflectivity of the surface starts to increase from the sapphire baseline value as the LT growth of GaN starts. Point 1 in the transient curve signifies the point where the LT growth is terminated and up-ramping of the temperature begins (see also Fig. 4.3). Although LT GaN has a relatively smooth surface morphology at this point of the process its crystal structure is mainly amorphous and disordered. As the temperature increases recrystallization of the LT GaN begins. Upon transition from LT to HT the disordered LT GaN NL partly decomposes [33]. A material redistribution process [34] leading to the formation of GaN islands accompanies the decomposition. During this redistribution process the surface morphology of the GaN film significantly roughens, as material concentrates into islands with a predominantly hexagonal crystal structure [34,35]. This leads to a rapid decrease in the surface reflectivity (point 2). As the temperature ramping continues the surface reflectivity starts to increase at point 3 in the curve. After this point the material redistribution process is dominated by desorption

and material loss from the hexagonal GaN islands leading to a partial exposure of the sapphire interface and a smoother surface morphology. The HT growth of GaN begins at point 4.
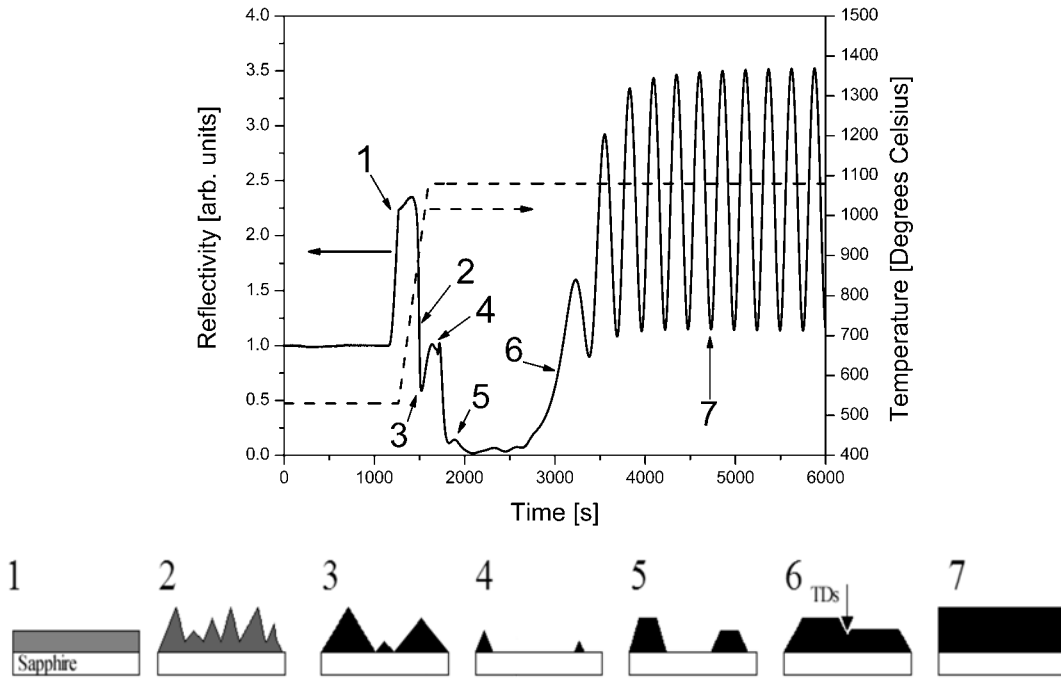
Figure 4.4. Growth model for GaN in the two-step process. The upper part of the illustration presents real reflectivity data obtained *in-situ* during two-step growth. The surface morphology corresponding to a point in the reflectivity transient is schematically presented in the lower part of the illustration.

During the beginning of HT growth nucleation occurs primarily on the hexagonal islands over the highly defective interfacial layer. These islands are henceforth referred to as nucleation islands (NIs). The 3D island growth makes the surface reflectivity decrease rapidly from point 4 on and reaches a minimum around point 5. After this point the lateral growth of the NIs gradually results in their coalescence. As the NIs merge the surface of the HT GaN film becomes smoother and its reflectivity starts increasing (point 6). Most TDs in a GaN film are formed at the coalescence boundaries of adjacent NIs, to accommodate for their relative crystalline misorientation [35]. After complete coalescence of the NIs film growth continues in a quasi-2D growth mode maintaining a smooth film surface. This leads to periodic oscillations (point 7) of the reflectivity transient due to interference effects as described in section 3.1.

4.4 Generation of dislocations

Given that the growth of GaN is based on heteroepitaxy the large lattice misfit between the substrate and the epilayer leads to a high density of dislocations. Various types of dislocations are generated during the two-step growth of GaN on c-plane sapphire. The resulting dislocation structure has been studied extensively [36,37].

During the LT NL growth on a nitridated surface small grains of hexagonal GaN are formed over the sapphire interface. The low growth temperature and the large lattice mismatch leads to a Volmer-Weber growth mode resulting in grain sizes in the order of 10 nm [38]. Following the recrystallization process as described in the previous section the NL is overgrown by HT GaN. During the island growth step before the coalescence of nucleation centers the NIs grow three-dimensionally (3D). Lateral growth of the islands occurs over the high-index planes and vertical growth occurs over the (0001) plane [39]. As the NIs overgrow the NL the stacking disorder between the NL and the predominantly hexagonal NIs is accommodated by stacking faults containing Frank and Shockley partial dislocations [35]. These dislocations have a line direction in the (0001) plane and do not thread through the film in the growth direction.

As HT island growth is continued for a sufficiently long time the NIs coalesce. Since the islands are somewhat misoriented relative to each other the majority of TDs is generated at the coalescence boundaries. In-plane twist between the NIs results in an edge component in the dislocation with the line direction along [0001]. Tilt misalignment results in a screw component (Burgers vector along [0001]) in the dislocations. Depending on the different directional components present in the dislocation they can be categorized as pure edge, screw or mixed type threading dislocations. On top of the highly faulted interfacial layer the large predominantly hexagonal islands contain only few screw or mixed type TDs. TDs generated at the boundaries of coalesced NIs are primarily edge-type. A schematic illustration of the dislocation generation process during two-step growth is shown in Fig. 4.5.
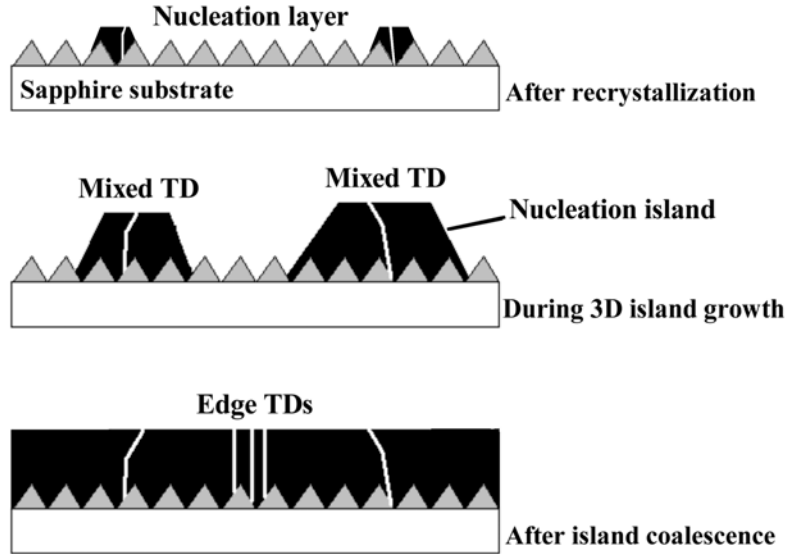
Figure 4.5. Threading dislocation generation during GaN growth.

4.5 Methods for high quality GaN growth

GaN films grown by the two-step method on c-plane sapphire can exhibit high TD densities. Depending on the optimization of process parameters the TD densities are in the range of 10^8-10^9 cm^{-2}. Although blue light emission has been demonstrated in structures where the TDD is over 10^{10} cm^{-2} the threading dislocations are known to cause detrimental effects on device performance. TDs can act as nonradiative recombination centers [40]. TDs can also reduce the lifetime of devices by acting as diffusion channels between electrodes [41]. For optoelectronic applications operating at high current densities further reduction of the TD density has become an essential part of research in the field of group III nitrides.

Epitaxial lateral overgrowth (ELOG) is an efficient method for suppressing threading dislocations in GaN by *ex-situ* sample manipulation [42]. In an ELOG process a few micrometers of GaN is first grown for example by the two-step process. Subsequently, an oxide mask (*e.g.* SiO$_2$) is deposited over the GaN surface. Photolithographic patterning of the mask is used to selectively expose regions of the underlying GaN layer. As more GaN is grown over the structure nucleation occurs exclusively on the exposed window regions and eventually the oxide mask is overgrown by GaN. The laterally grown sections of GaN over the mask grow relatively free of TDs. Overall TD densities in the order of 10^7 cm^{-2} are routinely obtained by the method [43]. Additionally, the masking process can be repeated several times to further reduce the TD density. The drawback of the ELOG technique is that it is *ex-situ* in nature. This makes the ELOG process very time consuming.

A popular *in-situ* method for the reduction of the TDD is SiN micromasking [44,45]. The principle of this method is similar to ELOG in the sense that a mask of different crystal structure is overgrown by GaN. The SiN mask is deposited using silane and ammonia as precursors in an MOCVD process on a GaN surface. The SiN layer incorporates nanoholes in the layer providing nucleation sites for GaN. Since the sticking coefficient of GaN on SiN is low GaN grows in a 3D mode over the mask. The TDs are not able to penetrate through the mask but are bent parallel to the (0001) surface [46].

5. Approaches for the reduction of the threading dislocation density

In this chapter the theoretical approaches into the reduction of the TDD in MOCVD grown GaN layers are briefly reviewed and a new approach is presented. The new approach emphasizes the shape, size and the distribution of NIs. The overgrowth of the NL and mechanisms responsible for the decrease in the TDD are also discussed.

Theoretically there exist three possibilities to control and reduce the TDD in lattice mismatched epitaxial layers. The first possibility is to prevent the generation of TDs. The theoretical considerations for the reduction of the generation of TDs are limited to reducing the density of nucleation centers. Experimental data supporting this approach to the reduction of TDD will be presented in chapter six. Another possibility is to force the TDs to move towards the sides of the layer at which they can be terminated. This can be in principle achieved by patterned substrates (pendeoepitaxy) [47] or by ELOG [43,48]. The third possibility is to provide a suitable environment for TDs to react among each other by fusion or annihilation [49].

TD reactions in (0001) oriented GaN layers have a much lower probability to occur than in (001) cubic semiconductor layers. In cubic semiconductors, TDs are inclined. This helps bringing them within a reaction distance from each other during layer growth [49, 50]. In (0001) oriented nitrides, practically all TDs have their line directions parallel to the growth direction. Therefore, the distance between TDs remains constant during growth [51] and no TD reactions are likely to occur. This thesis, however, suggests a new theoretical approach for TD density reduction in (0001) growth of GaN. The first stage to facilitate dislocation reactions proceeds via the externally forced dislocation inclination, which can be achieved for example by changing the growth mode to prefer inclined surface facets of nucleation centers. These facets are neither parallel nor perpendicular to the [0001] direction and they are characterized by high crystallographic plane indices {hk.l}. Hence the NL can be used to intentionally introduce surface roughness and to promote redirection of TDs.

Before a layer with a flat surface is formed, TDs are mostly terminated in the grooves between the neighboring NIs (see Fig. 5.1 a). In the case where 3D growth is sustained small neighboring islands are merged into larger ones, and some of the vertical TDs are terminated on inclined surfaces of the large islands. For these TDs, it is energetically

favorable to change their direction of propagation, provided that the energy barrier preventing inclination of the TDs is overcome (see Fig. 5.1 a). The inclination of TDs in the redirection layer is governed by diminishing the TD energy per unit length. This is feasible since TDs terminating perpendicular to an intentionally introduced high index facet plane are shorter compared to the TDs terminating with a line direction along the [0001] crystal axis. Previously, similar arguments were used in the analysis of the line trajectories of TDs in the growth of macroscopic crystals [52] to define the line directions of TDs in thin films [50] and to explain the bending of TDs during ELOG experiments [48].
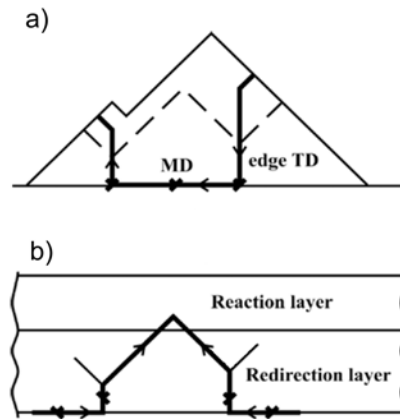
Figure 5.1. It is energetically favourable for threading dislocations to become inclined and perpendicular to the high-index facets of the NIs (a). Once inclined TDs thread within a reaction distance from each other they may annihilate (b) or fuse. The dashed lines in figure (a) signify the surface morphology of the layer at an earlier stage of growth illustrating the propagation of a TD in the grooves between neighboring NIs.

After the growth of the NL or "the dislocation redirection" layer the growth mode should be changed to prefer the flat (0001) surface in order to provide enough material volume for dislocation reactions. When the NL is overgrown, the inclined TDs retain their inclination. This causes the intersection points of TDs with the planar surface to move laterally across the surface. This effect was first explained in Refs. 49 and 50. As a result the probability of interaction between TDs significantly increases. This may lead to annihilation of two TDs (Fig. 5.1 b) or to fusion of two TDs to produce a single TD. Both of these processes provide a way to decrease the TD density.

The TD density can be quantitatively predicted by applying a reaction-kinetics model to the description of an ensemble of interacting TDs [49]. Simulations based on the presented model were used to predict the TDD in GaN layers as a function of film thickness [Publ. I]. The results are shown in Fig. 5.2.
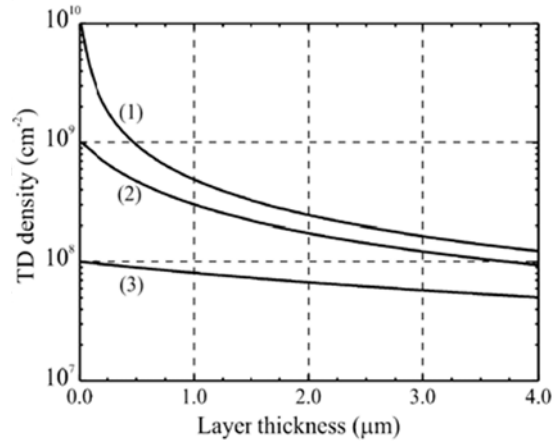
Figure 5.2. Simulated results for TD density vs. layer thickness [Publ. I]. The results are plotted for initial TD densities of (1) 10^{10} cm^{-2}, (2) 10^9 cm^{-2} and (3) 10^8 cm^{-2}.

6. The multistep growth method

This chapter presents the experimental part in the development of the new growth method to decrease the TD density in GaN films. Optimization of the properties of a NL is discussed with the emphasis being on reduction of the NI density. The latter part of this chapter focuses on HT overgrowth of the NL. The theoretical discussion about the method was presented in Chapter 5.

6.1 Growth of GaN islands

The possibility to accurately change the size and shape of nucleation centers for a subsequent HT growth step would be of help in controlling the morphology of the NL. To this end a series of GaN NLs were grown by alternately depositing a thin layer of LT GaN and annealing this film for recrystallization. The *in-situ* reflectometry data of Fig. 6.1 were recorded during a process in which four cycles of LT growth and recrystallization were used to synthesize GaN NIs. In the inset of Fig. 6.1, the critical points of the reflectivity curve of one cycle of LT deposition and recrystallization are labeled. The shape of this curve is typical for LT-GaN deposition followed by an annealing step [34,53]. Film deposition occurs between points 1 and 2 as predominantly cubic (111) oriented GaN is grown [35,53,54]. During this time the reflectivity increases due to constructive interference between the wavefront reflected from the film surface and the wavefront reflected from the GaN-sapphire interface. After the interruption of film growth the slower increase in reflectivity from point 2 on is caused by the increase in the refractive index of GaN as a function of temperature. This increase in reflectivity takes place during the beginning of the temperature up-ramping step (between points 2 and 4) until point 3 is reached. As temperature up-ramping is continued beyond point 3 island formation starts at approximately 900 °C. This event is accompanied by surface roughening causing the reflectivity to decrease. Point 4 in the reflectivity transient of Fig. 6.1 signifies the time at which temperature down-ramping begins. From this point on the reflectivity of the sample surface remains essentially unchanged before the next deposition cycle.
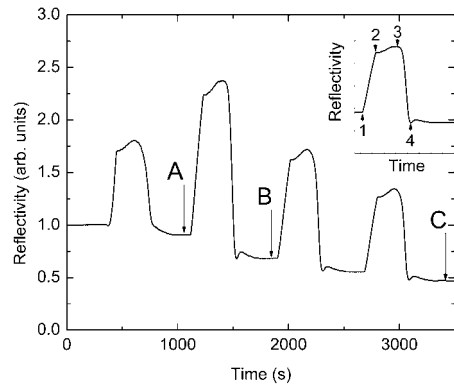
Figure 6.1. Surface reflectivity during the multistep growth of GaN nucleation islands [Publ. II].

As can be seen in Fig. 6.1, the minimum stabilized reflectivity during a temperature down-ramping gradually decreases after each cycle reaching a minimum of about 0.5 at point C. This trend is due to increase in the size of GaN islands as depicted in the AFM micrographs of Fig. 6.2 a, b and c. These images illustrate the surface morphology of the samples X, Y and Z, which were grown with one, two and four LT deposition and recrystallization cycles, respectively. In the reflectivity curve of Fig. 6.1 these samples correspond to points A, B and C, respectively. The AFM measurements suggest that the density of islands remains virtually unchanged at about 6×10^7 cm^{-2} after each cycle. Also, the background roughness in between the islands is similar for each sample. The average height of the islands in the samples X, Y and Z is 135 nm, 375 nm and 410 nm, respectively, indicating that island growth in the [0001] direction saturates after two cycles of LT GaN deposition. The increasingly large flat area on top of most of the islands also suggests that the (0001) surfaces become stabilized after the growth has saturated in the [0001] direction. Similar results have been reported elsewhere [54].
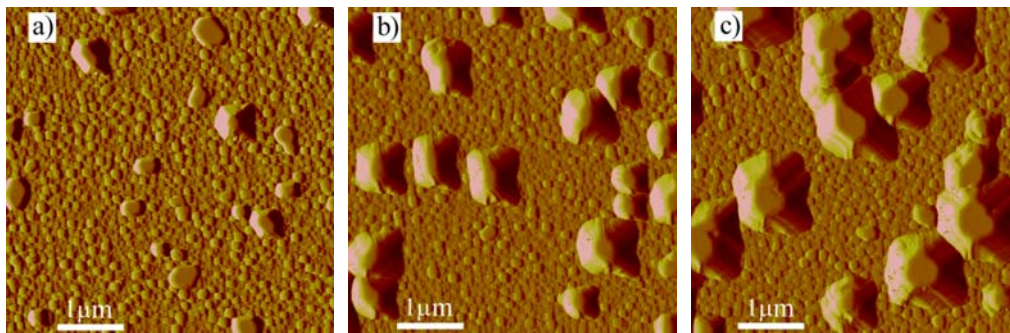
Figure 6.2. AFM data illustrating the surface morphology for the samples grown with one (a), two (b) and four (c) multistep cycles [Publ. II]. The images were obtained in deflection mode.

Further calculations based on the measured AFM data show that nominally about 5-10 nm of film is contained in the GaN islands in the sample X. The corresponding nominal film thickness for islands in the samples Y and Z are about 50 nm and 110 nm, respectively. These results were obtained from the AFM height data with computer software by numerically calculating the volume of material that is contained in the nucleation islands and averaging this volume over the scanned 25 μm^2 area. The volume was also calculated by modeling the islands as cylinders having a diameter equal to the full width at half of the maximum height of an island. The results from these two methods were the same within an error of a few nanometers of nominal film thickness. Since, based on the growth rate used, about 33 nm of LT GaN is deposited in each cycle, we can conclude that during recrystallization virtually all of the deposited film nucleates on the existing islands formed during the previous recrystallization step.

The dark field cross-sectional TEM data of Fig. 6.3 shows the cross-sectional profile of the deposit in between the GaN nucleation islands in the sample Z. Calculations based on the data gives an average thickness of about 15-20 nm for this thinner deposit forming the background of the AFM images in Fig. 6.2. The result suggests that very little or none of the deposited LT material is lost by desorption during the recrystallization process. The measurements and calculations above support the observations by Lada and co-workers [34].
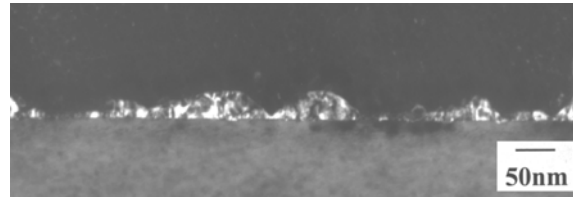
Figure 6.3. TEM data illustrating the thin interfacial layer in between the NIs in the sample Z [Publ. II].

The crystal quality of the samples X, Y and Z was evaluated from the XRD data of Fig. 6.4. These measurements were carried out in a triple-axis configuration for maximum resolution. The 2theta-omega curves around the peak of the (0002) symmetrical reflection for hexagonal GaN are shown in the figure. The FWHM (Full Width at Half Maximum) of these peaks for the samples X, Y and Z were 215.3, 202.0 and 186.1 arcsec, respectively. Narrowing of the (0002) diffraction peaks is accompanied by a significant increase in the diffracted intensity as the number of LT-GaN deposition cycles increases and the proportion of the material contained in the islands is increased. These observations suggest that the material, which nucleates on existing GaN islands during the recrystallization step of each cycle, has a smaller density of dislocations with a screw component than the thinner deposit contained in between the islands [35,55]. Additionally, the more pronounced hexagon-shaped plan-view cross-section of the

islands in the sample Z (Fig. 6.2 c) would loosely indicate that the redeposited material is of better crystal quality in general than the film in between islands; an argument also supported by previous studies indicating that good quality hexagonal GaN is regrown on the nucleation centers during the recrystallization step [34]. Further evidence for this statement is provided in the bright field cross-sectional TEM data of Fig. 6.5 taken from the sample Z. This is a bright field image and it was taken with the substrate tilted about 4 degrees away from the [2110] zone normal in the [0110] direction. This image indicates a region of higher density of defects, labeled as E, under the island. The defects are well confined within a region close to the sapphire interface. The thickness of this region is roughly the same as the thickness of the thin deposit in between the islands. A region of higher defect content is also contained within the island but is well confined within a boundary labeled as U. The outer regions of the island have less contrast variations suggesting smaller defect content.
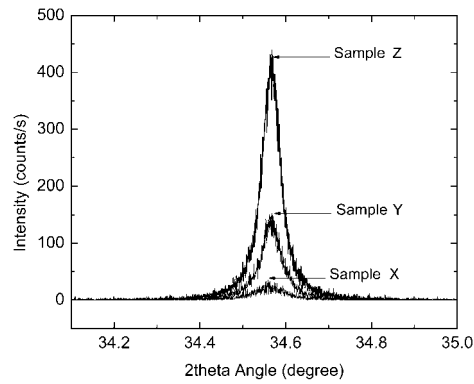
Figure 6.4. XRD data from a (0002) 2theta-omega scan for GaN. The curves represent data for the samples X, Y, and Z illustrated in Figs. 6.2 a, b and c respectively [Publ. II].
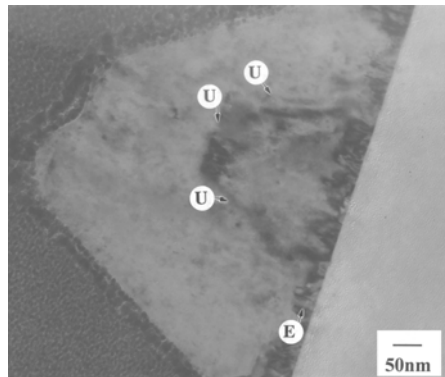
Figure 6.5. TEM data obtained from a NI in the sample Z (see Fig. 6.2 c) [Publ. II]. The image is tilted to fit the frame.

30

Ref. 56 reports that shorter deposition times for the LT NL results in reduced NI density after HT treatment and recrystallization of the LT layer. The multistep method takes advantage of this phenomenon as it can be used to increase the size of NIs without affecting their density. This enables the deposition of very thin LT NLs and the further reduction of the NI density while keeping the size of NIs sufficiently large for them to efficiently act as nucleation centers during the HT overgrowth of the NL. The surface morphology of four GaN NLs is presented in the AFM micrographs of Fig. 6.6. The NL in Fig. 6.6 a (sample A) was prepared with the standard "one-cycle" method by depositing approximately 50 nm of LT film at 530 °C and subsequently up-ramping the temperature to 1060 °C for recrystallization. After this the temperature was ramped down back to 530 °C again. The growth process for the samples in Figs. 6.6 b, c and d (samples B, C and D, respectively) consisted of two, three and four process cycles, respectively. The total nominal thickness of deposited material was approximately 50 nm for each of the three samples. Thus, the thickness of the LT film deposited in each cycle of the multistep process was 25 nm, 17 nm and 13 nm for the samples B, C and D, respectively. The annealing steps were identical to the one used during the growth of the sample A. The presented AFM data indicates a substantial decrease in the NI density. The NI density for the samples A, B, C and D as calculated from Fig. 6.6 is $1.1 \times 10^8\,\mathrm{cm}^{-2}$, 7.4×10^7 cm^{-2}, $4.5 \times 10^7\,\mathrm{cm}^{-2}$ and $1.7 \times 10^7\,\mathrm{cm}^{-2}$, respectively. This is among the best results reported thus far as obtained by *in-situ* methods. Previously, SiN_x *in-situ* micromasking techniques have resulted in NI densities of over $10^8\,\mathrm{cm}^{-2}$ [57].
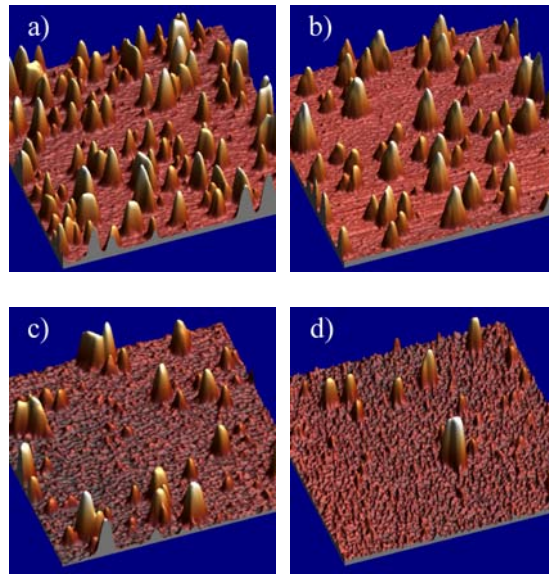
Figure 6.6. AFM data illustrating the NI density of recrystallized GaN NLs. Nominally 50 nm of LT film was deposited in one (a), two (b), three (c) and four (d) cycles [Publ. III].

The reason behind the drastic reduction in NI density is most likely related to the diffusion mechanisms governing the material redistribution process during an annealing

step. It has been suggested that the substantial mass transport responsible for the islanding could be explained by the formation of either weaker N-Ga bonds between partially dehydrogenated NH_3 molecules and the GaN surface [58] or by the migration of Ga-N molecules on a Ga-terminated surface [59]. Given that the diffusion lengths and lifetimes of the intermediate species can be extremely large [58] we believe that surface diffusion is not the limiting factor in decreasing the NI density. Rather, a gas phase diffusion process determines the density of nucleation sites during recrystallization. This argument is supported by previous studies [60] indicating that in addition to decomposition and subsequent surface diffusion, Ga reincorporation through the gas phase into the GaN islands is responsible for their formation. A symptom of this mass transport process is the formation of hexagonal caps on top of disordered material during growth of the NIs as reported in Refs. 34 and 61. When the thickness of the LT GaN film deposited before an annealing step decreases so does the volume of material decomposing during annealing. Subsequently, the amount of material reincorporated into the film through gas phase becomes smaller resulting in fewer nucleation sites on the NL and consequently to smaller NI densities.

The nominal thickness of material contained in the NIs was 32 nm, 39 nm, 11 nm and 3 nm for the samples A, B, C and D, respectively. Based on the study in publication II the nominal NL thickness in between the islands can be assumed to be roughly equal, about 15-30 nm, in each sample. This result suggests that a significant amount of material is lost due to desorption in the samples C and D. This type of material loss does not occur when thicker LT GaN films are recrystallized [34] since more nucleation sites are available for molecules diffusing on the film surface. Assuming that the diffusing molecules have a limited residence time on the film surface their probability of desorption increases with increasing diffusion distance.

Although we have demonstrated significant reduction in NI density using the multistep NL method, one should also be able to control the overgrowth of the NL in order to prevent new islands from forming during the HT growth step. Keeping this in mind we have studied the effect of carrier gas flow rate and total reactor pressure on the evolution of film morphology during the initial stages of HT NL overgrowth. The AFM data in Figs. 6.7 a, b, c and d illustrate the surface morphology for the samples E, F, G and H, respectively. The growth process for these samples consisted of first growing a NL with a reduced NI density, similar to the sample D (Fig. 6.6 d). This NL was subsequently overgrown at HT for 300 s in the samples E, F, G and for 700 s in the sample H. The total hydrogen flow rate and reactor pressure were 10.5 slm and 200 torr for the sample E, 10.5 slm and 400 torr for the sample F and 12 slm and 500 torr for both of the samples G and H. The HT overgrowth temperature was 1060 °C for each sample.

Figs. 6.7 a and b clearly indicate how the increase in reactor pressure reduces nucleation in between the sparse NIs obtained by the multistep process (Fig. 6.6 d). The GaN island density, of about 3.0×10^7 cm^{-2} in the sample F is still substantially higher than the original NI density in the sample D. Increasing the total pressure and carrier gas flow rate up to 500 torr and 12 slm, respectively, further reduces nucleation in between the original NIs. This can be observed from the sample G (Fig. 6.7 c), where the island density is

about 1.7×10^7 cm^{-2} corresponding to the original NI density in the sample D. As the NL overgrowth is continued for 700 s it can be observed that the island density remains constant (Fig. 6.7 d) at 1.7×10^7 cm^{-2} and the growth occurs selectively on the largest islands.
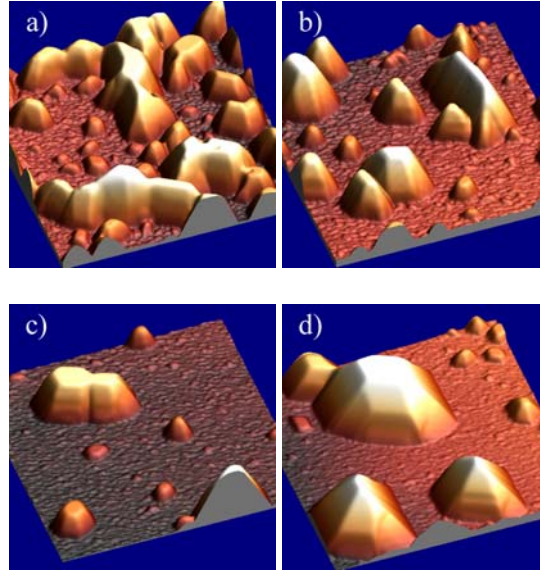
Figure 6.7. AFM data illustrating the surface morphology of GaN films in the beginning of HT overgrowth. The samples in a, b and c were overgrown for 300 s and the sample in d was overgrown for 700 s [Publ. III].

It has been previously reported that increasing reactor pressure enhances GaN decomposition in a H_2 atmosphere [62]. The phenomenon has been exploited in the work of Chen *et al.* [63] who reported a decrease in the size of nucleation sites (this should not be misinterpreted as a reduction in NI density) as process pressure was increased for the growth of a LT GaN NL. We suggest that the improved nucleation selectivity at higher pressures during the overgrowth of NLs with an extremely low NI density is caused by faster decomposition of the thermally more unstable film in between the NIs. The suppression of nucleation in between the NIs can be further improved by increasing the H_2-carrier-gas flow as we have done for the samples G and H. This will potentially increase the amount of reactive hydrogen on the film surface required for the GaN decomposition (etching) reaction forming NH_3 [62].

6.2 Overgrowth of the nucleation layer

The fundamental reason for the experimentally observed high TD density in GaN layers is the high density of nucleation sites generated during the growth of the NL [64,35]. This

suggests that the multistep NL growth presented in the previous section should enable a reduction in TDD.

GaN buffer layers were grown to evaluate the ability of the multistep NL technique to reduce the density of TDs. The growth process for each sample was identical after completion of the NL, *i.e.*, after the last recrystallization step. The overgrowth of the NL was optimized for reduced threading dislocation density [65] in the studied GaN buffer layers. To evaluate the TD density the samples were etched in a mixture of phosphoric and sulfuric acids after the growth process. The density of etch pits was then measured by AFM. Fig. 6.8 illustrates the AFM data from two 2.3 μm thick GaN films with etch pits on their surface. Fig. 6.8 a shows the etch-pit density (EPD) of the sample I grown by the standard two-step method. Fig. 6.8 b is an EPD scan from the sample J in which the multistep technique was used to grow the NL similar to the sample B. The calculated EPD was 2.0×10^8 cm^{-2} and 1.0×10^8 cm^{-2} for the samples I and J, respectively. By comparing this result with the NI density for the samples A and B we observe that the EPD and, therefore, the TD density decrease roughly in proportion with the NI density of the NL.
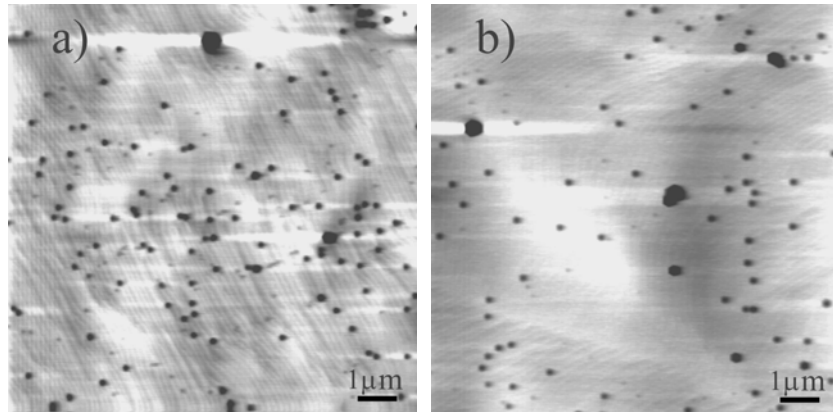
Figure 6.8. AFM data presenting the EPD of GaN layers grown by the two-step method (a) and the multistep method (b) [Publ. III].

Fig. 6.9 presents XRD data measured from the samples in Fig. 6.8. The data was obtained from the asymmetric (302)-diffraction. Rocking curve (ω scan) and 2θ-ω data were recorded for both samples. These scans indicate a clear improvement in the crystal quality for the multistep sample. The rocking curve FWHM peak widths in Fig. 6.9 a are 363 arcsec and 251 arcsec for the standard and the multistep sample, respectively. The result suggests that the TD content is significantly reduced in the GaN film due to the multistep NL [66]. Furthermore, according to the Scherrer formula [67] the coherence lengths in a crystal can be estimated from the peak widths of a 2θ-ω scan. The FWHM of these peaks is inversely proportional to the coherence length. The 155 arcsec and 113 arcsec peak widths in the 2θ-ω scan data of Fig. 6.9 b correspond to a 37% increase in the coherence length for the multistep sample. In light of our previously reported results

about the reduction in NI density by the multistep technique the increase in coherence length is expected; smaller NI density leads to larger grains (Fig. 6.7 d) and increased coherence in the film.
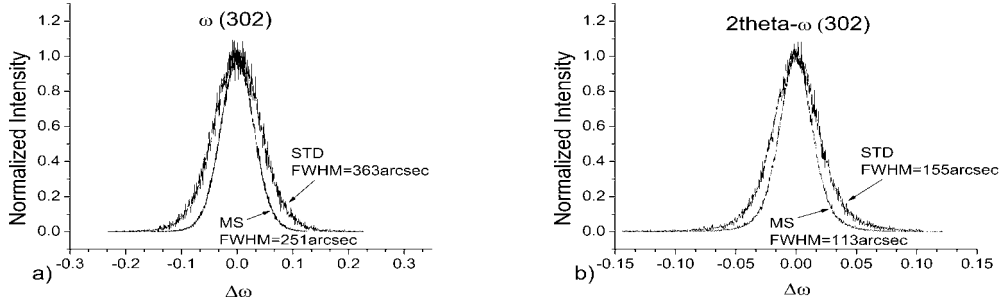
Figure 6.9. Rocking curve (a) and 2theta-omega (b) XRD data from the GaN films presented in Fig. 6.8 [Publ. III].

6.3 Redirection and reactions of threading dislocations

A new approach for the enhancement of reactions between TDs was presented in chapter 5. As a further improvement to the multistep method, the sparse 3D NIs were overgrown with a suitable set of process parameters to stimulate high-index facet growth of these nucleation centers [Publ. IV]. A TMGa molar flow rate of 200 μmol/min and an ammonia flow rate of 3 slm were used during the beginning of HT overgrowth. The V/III ratio was subsequently increased to 800 in order to promote island coalescence and the resulting dislocation reactions. The increase in V/III ratio additionally stimulates 2D growth and eliminates surface roughening. The NIs were overgrown at HT for 300-700 s in a pressure of 200-500 torr with a hydrogen flow rate of 10-12 slm.

In the frame of the proposed approach, it is expected that a low NI density enable prolonged vertical growth of NIs before their coalescence. As a result more pronounced TD inclination is likely to occur. Cross-section transmission electron microscopy (TEM) was used to determine the orientation of TDs inside a NI overgrown at HT with a low V/III ratio. The measured sample was grown in a process, which was interrupted prior to the coalescence of NIs. The TEM data are shown in Fig. 6.10. In the figure one can clearly observe that an essential part of the TDs incline from the [0001] direction and become perpendicular to a high-index facet of the NI. This type of inclination of TDs inside NIs has not been previously demonstrated.
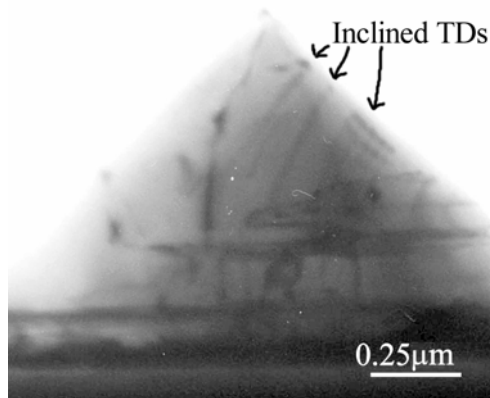
Figure 6.10. TEM data illustrating the inclination of TDs inside a GaN NI [Publ. IV].

To evaluate TD density in the grown layers the samples were etched in a mixture of phosphoric and sulfuric acids after the growth process. The density of etch pits was then measured by AFM. Fig. 6.11 illustrates the AFM data for two 2.3 μm thick GaN films with etch pits on their surface. Fig. 6.11 a shows a scan from a sample grown by the standard two-step method. The NI density for this sample was 1.6×10^8 cm^{-2}. Fig. 6.11 b is an AFM scan from a sample grown by the multistep process. For this sample the NI density was about 5×10^7 cm^{-2} and no surface roughening of the buffer layer was observed. The calculated EPD was 1.4×10^8 cm^{-2} and 5.0×10^7 cm^{-2} for the standard sample and for the multistep sample, respectively. The AFM data were supported by plan-view TEM measurements, which directly reveal the points where dislocation lines are terminated at the surface. The result of these measurements for the sample of Fig. 6.11 b is shown in Fig. 6.12. A TD density of about 5.0×10^7 cm^{-2} in the GaN epilayer can be calculated from the image.

The experimentally obtained TD density of 5.0×10^7 cm^{-2} is in good agreement with the simulated result of chapter 5 taking into account the interactions between inclined TDs. Additionally, in Fig. 6.11 b two sizes of etch pits can be identified. This is a result of the crystallographic selectivity of the etching chemical causing different etching rates for TDs with different Burgers vectors [68,22]. Fig. 6.11 b indicates that the etch pits are virtually all of the smaller type. We suggest that the very few larger etch pits result from yet unreacted inclined TDs generated inside NIs [35]. This suggestion is compatible with the plan-view TEM data of Fig. 6.12 showing that TDs reaching the film surface are all of the vertical edge type. Vertical edge type TDs are known to form primarily in between the coalescence boundaries of NIs [35]. Hence Fig. 6.12 provides further support to the assumption that the inclined TDs originating from NIs do not propagate through the film but rather react with each other.
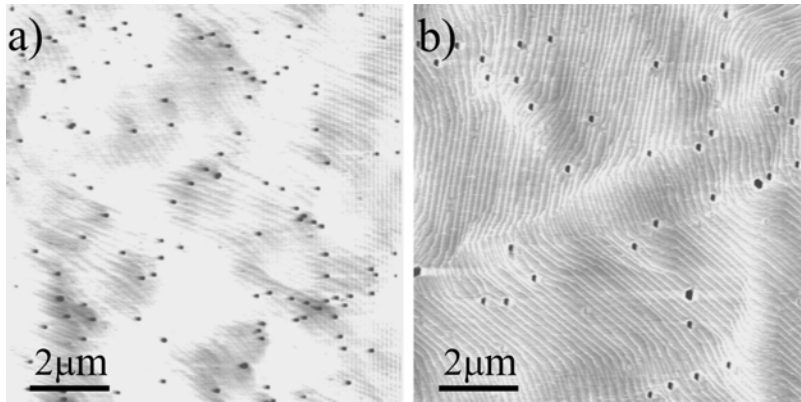
Figure 6.11. AFM data illustrating the EPD on GaN layers grown by the two-step method (a) and the multistep method (b). A low V/III ratio was used during the beginning of HT growth for both samples to stimulate inclination of TDs [Publ. IV].
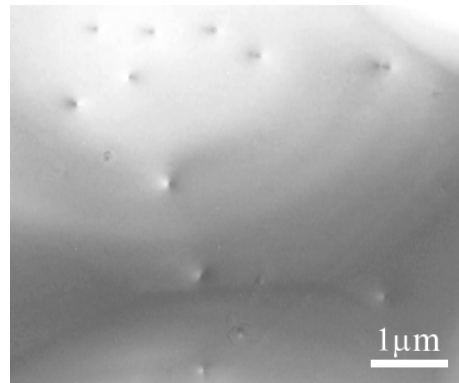
Figure 6.12. Plan-view TEM data from the sample of Fig. 6.11 b [Publ. IV].

As an example to demonstrate the effect of the multistep growth of the GaN buffer on the performance of optoelectronic devices two LED structures were fabricated. These LEDs had a multiple quantum well (MQW) active region with 10 quantum wells. The buffer layer for one LED was grown by the conventional two-step method (TDD=$6x10^8$ cm^{-2}). For the other LED, the newly developed multistep method was used to reduce the TDD (TDD=$7x10^7$ cm^{-2}) in the GaN buffer. Apart from this difference in the template quality the growth process and post-growth processing were identical for both devices. The LEDs had the emission peak at the wavelength of 460 nm. The cross-sectional area of the active region was 1 mm^2 for each device. Fig. 6.13 illustrates the behavior of the output light intensity for the two LEDs as a function of the operating current. The data indicates, as expected, that the lower TDD provided by the multistep GaN template decreases the saturation in the light intensity when the devices are driven at higher electrical power. The details of this study can be found in publication VI.
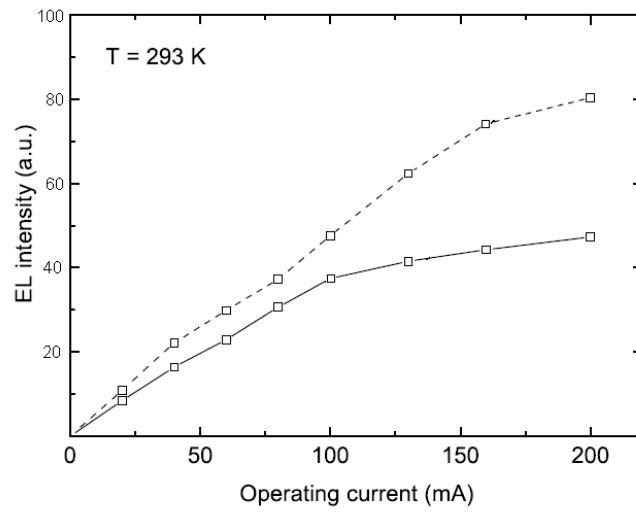
Figure 6.13. Electroluminescence data from two LEDs. The dashed (solid) line corresponds to the device grown on the template with a lower (higher) TDD resulting from the multistep (conventional two-step) method.

7. The multistep growth method for AlGaN

This chapter of the thesis discusses how the multistep MOCVD growth method for GaN can be adopted to synthesize AlGaN layers with a reduced TD density.

Several attempts have been previously made in order to use a LT NL for the growth of AlGaN [69,70]. The use of Al already in the LT film is preferable. This would enable the growth of a wide bandgap layer at the substrate interface helping the design of optoelectronic devices operating at UV and deep UV wavelengths. However, this type of crystal growth for AlGaN has several difficulties. The slow surface diffusion of the Al species in the MOCVD processes for group III nitrides results in a very high density of small NIs after recrystallization of an Al containing LT NL [69]. Additionally, island growth of high temperature AlGaN is more difficult to obtain. Consequently, island coalescence occurs very rapidly when HT AlGaN growth is started and the high density of coalescence boundaries results in TD densities of around 10^{10} cm^{-2} [71]. On the other hand, if a GaN buffer layer is utilized to improve the AlGaN quality the lattice mismatch between GaN and AlGaN can result in cracking of the AlGaN epilayers [71].

Several growth techniques have been developed to decrease the TD density in AlGaN films. These techniques include pendeoepitaxy and various epitaxial lateral overgrowth (ELOG) methods [72,73,74]. Although the TD density can be decreased by these methods they are very time consuming, as *ex-situ* sample manipulation is required. The new multistep method for AlGaN growth takes advantage of the good surface diffusivity of the Ga species on a nitrogen-terminated surface [58]. This enables the growth of GaN NIs with a small density by several consecutive process cycles where LT GaN is deposited on top of recrystallized GaN islands. The details of this stage of the process are described in publication III. Fig. 7.1 illustrates the surface reflectivity of a sample during a multistep AlGaN process where four process cycles were used for the growth of GaN NIs. The reflectivity was measured *in-situ* in normal incidence geometry at a wavelength of 638 nm. The growth of HT GaN was started after the growth of GaN NIs at point A in Fig. 7.1. Surface roughening due to the 3D growth of GaN NIs causes the rapid decrease in the surface reflectivity between points A and B in the curve. The surface morphology of the sample at point B is presented in the AFM data of Fig. 7.2. It can be seen that at this point of the process the 3D growth of GaN has reached a stage where the NIs have not yet coalesced and they form a discontinuous GaN film. When the HT AlGaN growth starts (point B in Fig. 7.1) the reflectivity begins to oscillate with a small but increasing amplitude. This suggests that AlGaN grows relatively uniformly over the GaN NIs and in

the pits in between the NIs. The situation is different from the one observed in HT GaN growth where complete island coalescence results in a large increase in the surface reflectivity before the beginning of strong interference effects and oscillations [53]. Finally, the surface reflectivity starts to increase asymptotically after point B as the surface of the AlGaN film becomes smoother.
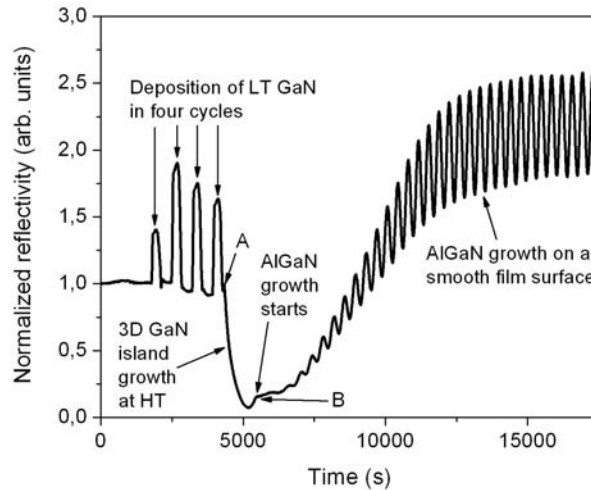
Figure 7.1. Surface reflectivity of a sample during the multistep AlGaN process. Four process cycles were used for the growth of GaN NIs [Publ. V].
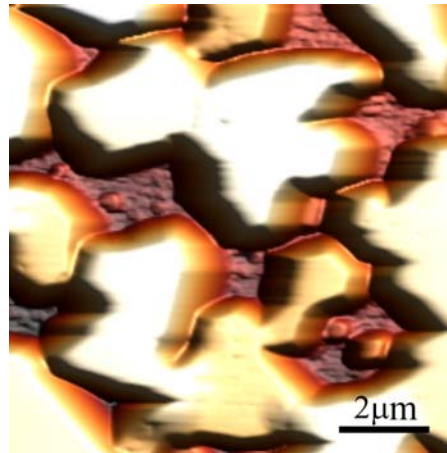
Figure 7.2. Surface morphology of the GaN NL prior to the beginning of the HT AlGaN growth step. The 3D growth of GaN has reached a stage where the NIs have not yet coalesced and they form a discontinuous GaN film [Publ. V].

40

As we have demonstrated in section 6.1 the NI density can be significantly decreased when the NL is deposited during several LT growth steps. Due to the smaller NI density we are able to use a prolonged coalescence period before the individual NIs merge. This period can be used to promote the inclination of TDs inside GaN NIs by suitably controlling the shape of the islands as presented in publications I and IV. In practice this is done by using a low V/III ratio during the HT GaN growth. The multistep method for AlGaN growth was used to optimize the growth of crack-free $Al_{0.12}Ga_{0.88}N$ layers with a thickness of 2 μm. Two LT deposition cycles were used to grow the GaN NL with a small NI density of $6x10^7$ cm^{-2}. Subsequently, nominally 300 nm of HT GaN was grown over the GaN nucleation islands to increase their size. The growth of $Al_{0.12}Ga_{0.88}N$ was started when the GaN NIs approached coalescence as described above (see Fig. 7.2).

To demonstrate the effect of the new multistep method on the TD density of AlGaN layers several $Al_{0.12}Ga_{0.88}N$ films were grown with varying V/III ratios in the HT GaN growth step. The samples illustrated by the AFM data of Fig. 7.3 went through wet chemical etching before the AFM measurement in order to bring out TDs as etch pits. For the sample in Fig. 7.3 a (sample A) a V/III ratio of 1500 was used during the HT GaN growth step. For the sample in Fig. 7.3 b (sample B) the V/III ratio was decreased to 450 to promote the vertical growth of the NIs and the resulting TD inclination. The calculated etch-pit density (EPD) for the sample A and the sample B was $2.8x10^9$ cm^{-2} and $5x10^8$ cm^{-2}, respectively. Previously *ex-situ* techniques such as ELOG or pendeoepitaxy have been required to obtain such low TD densities in $Al_{0.12}Ga_{0.88}N$ buffer layers grown on a thin GaN NL.
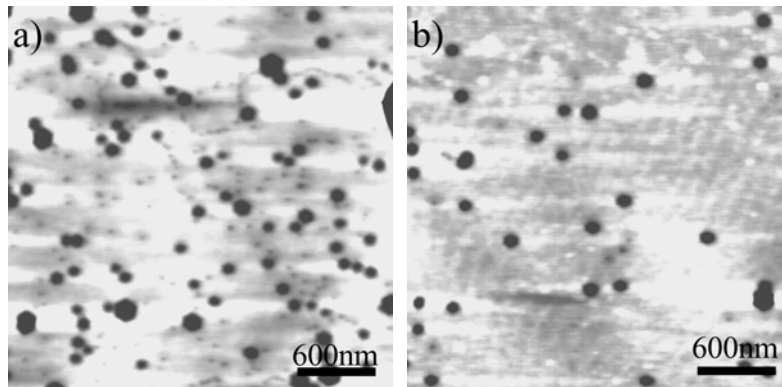
Figure 7.3. AFM scans showing the etch pits on the surface of a) the sample A and b) the sample B. The decrease in V/III ratio for HT AlGaN growth significantly reduced the EPD [Publ. V]. The scale of the figures is 3 μm x 3μm.

The result of improved crystal quality suggested by the EPD data is supported by the HR-XRD data from the samples in Fig. 7.3. This data is illustrated in Fig. 7.4 presenting the (002) and (302) rocking curve diffraction peaks for the $Al_{0.12}Ga_{0.88}N$ layers. The full width at half maximum (FWHM) of the diffraction peak for the sample A and for the sample B in the (002) diffraction was 390 arcsec and 270 arcsec, respectively. The

corresponding values in the (302) diffraction were 840 arcsec for the sample A and 420 arcsec for the sample B. The results demonstrate that the multistep method for AlGaN growth can be efficiently utilized to decrease TD density and to improve the crystal quality in thick and crack-free AlGaN epilayers. Based on the presented data the mechanisms responsible for the drastic reduction in the TD density can be assumed to be similar to the ones reported previously for the multistep GaN growth.
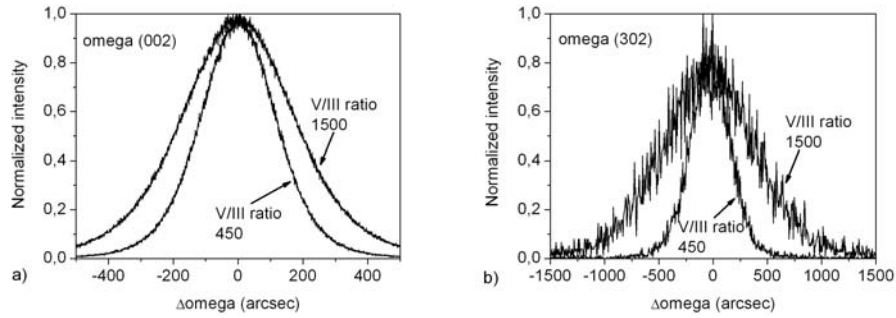
Figure 7.4. HR-XRD data for the samples A (V/III=1500) and B (V/III=450). The AlGaN diffraction peaks in a) the (002) and b) the (302) diffraction are illustrated [Publ. V].

One of the benefits of using a thin LT NL on sapphire as the starting surface for AlGaN growth is that the theoretical critical thickness of an AlGaN layer on GaN can be substantially exceeded [69]. The cross sectional TEM data in Fig. 7.5 from the sample A illustrates that bundles of TDs are generated at regions where $Al_{0.12}Ga_{0.88}N$ grows directly on top of the highly defective interfacial layer on the sapphire substrate. These are the regions in between the GaN NIs that are exposed for AlGaN growth after the HT GaN growth step. Relaxation of films through the generation of TDs at the exposed regions helps to explain the crack-free growth of the studied $Al_{0.12}Ga_{0.88}N$ layers. The result is in agreement with previous observations indicating that thick AlGaN layers can be grown crack-free either directly on a sapphire substrate or on a thin LT NL [75].

TDs are also able to relax stresses in a heteroepitaxial film by inclination from the vertical growth direction [76]. We suggest that when penetrating into the overgrowing $Al_{0.12}Ga_{0.88}N$ layer some of the TDs are able to retain their inclination further enhancing the relaxation of the film. Detailed behavior of TDs at the interface between GaN NIs and the overgrowing AlGaN layer will be a topic for future research.
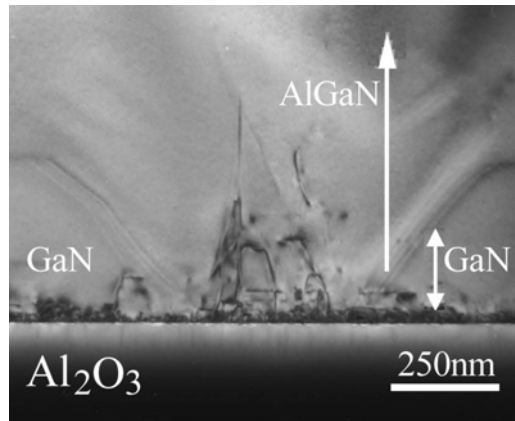
Figure 7.5. TEM data illustrating TDs generated at regions where $Al_{0.12}Ga_{0.88}N$ grows directly on top of the highly defective interfacial layer on the sapphire substrate [Publ. V].

8. Summary

The development of the widely used two-step MOCVD growth procedure for GaN on c-plane sapphire has been a critical step towards commercial GaN-based optoelectronics. The benefits of this method are limited by the high density of threading dislocations in the grown films. Substantial research has been carried out in order to reduce the TD density either by reducing the density of nucleation centers or by forcing the TDs to bend parallel to the film surface.

In this thesis a novel theoretical approach for the TD density reduction in MOCVD grown GaN layers was discussed. The approach relies on the ability of inclined TDs to react with each other by annihilation or fusion. Inclination of TDs can be stimulated by deliberately introducing surface roughness on the growing film. This gives TDs the possibility to minimize their energy by deviating from the [0001] direction.

Reduction in the density of nucleation centers can be done by *in-situ* or *ex-situ* masking of the growing GaN layer. This thesis presented a new MOCVD growth method, which can be utilized to drastically reduce the density of nucleation centers *in-situ* on a GaN NL without using any masking material. The method involves alternate deposition of a thin LT layer and recrystallization of this layer in a multistep process. EPD, TEM and HR-XRD measurements were used to demonstrate the effect of the developed method on the TD density.

In addition to providing a lower density of coalescence boundaries the reduced NI density enables a longer growth period before coalescence of individual islands. This period could be utilized for 3D growth of GaN NIs to introduce surface roughness. In light of our theory the 3D growth stimulates inclination of TDs resulting in enhancement of their mutual reactions and in a decrease in the TD density. These results were experimentally confirmed by EPD and TEM measurements. By combining the effects of reduced NI density and inclination of TDs inside the NIs a TD density of down to 5×10^{7} cm^{-2} was obtained. In general we have shown that an *in-situ* MOCVD process without micromasking can produce GaN films on c-plane sapphire with a TD density comparable to the values obtained by *ex-situ* techniques such as ELOG.

The multistep growth process was adopted for the growth of AlGaN. The method exploits the good surface diffusivity of the Ga species on a nitrogen-terminated surface to grow a sparse distribution of NIs. HT growth of AlGaN starts prior to the coalescence of the NIs

enabling the penetration of the Al species to the substrate interface. The growth of AlGaN on a discontinuous GaN NL further enabled relaxation of $Al_{0.12}Ga_{0.88}N$ epilayers. The relaxation occurred through dislocations generated at the exposed areas of the substrate interface in between the GaN NIs.

The multistep AlGaN process enabled a reduction in the TD density by exploiting similar mechanisms for TDD reduction as the multistep process for GaN. These mechanisms were the reduction of the NI density and promotion of inclination of TDs inside the NIs. A TD density of down to $5x10^8$ cm^{-2} for crack-free $Al_{0.12}Ga_{0.88}N$ layers was reported.

Further research in the area of this thesis should include *e.g.* the combination of *in-situ* SiN micromasking and the multistep method. If successful this approach would further reduce the TD density in group III nitride epilayers still keeping the process *in-situ* in nature. The applicability of the multistep method on other foreign substrates such as SiC should also be investigated. More TEM studies are needed to gain insight about the reactions between inclined TDs. For laser applications, the luminescence properties of GaN-based structures prepared on the high quality multistep templates should be studied under high intensity pumping conditions and high injection currents. Finally, with efficient UV emitters in mind, the incorporation of more Al into the AlGaN layers prepared by the multistep method should be an interesting topic for further research.

References

[1] I. Akasaki, H. Amano, Y. Koide, K. Hiramatsu, N. Sawaki, J. Cryst. Growth 98 (1989) 209.

[2] H. Amano, M. Kito, K. Hiramatsu, I. Akasaki, Jpn. J. Appl. Phys. 28 (1989) L2112.

[3] S.Nakamura, Jpn. J. Appl. Phys. 30 (1991) L1705.

[4] S. J. Pearton, J. C. Zolper, R. J. Shul, F. Ren, J. Appl. Phys. 86 (1999) 1.

[5] S. Nakamura, G. Fasol, *The Blue Laser Diode*, Springer Verlag, Berlin Heidelberg New York, 1997.

[6] J. Neugebauer, phys. stat. sol. (b) 227 (2001) 93.

[7] A. Smith, R. Feenstra, D. Greve, M. Shin, M. Skowronski, J. Neugebauer, J. Northrup, Surf. Sci. 423 (1999) 70.

[8] O. Ambacher, B. Foutz, J. Smart, J. Shealy, N. Weimann, K. Chu, M. Murphy, A. Sierakowski, W. Schaff, L. Eastman, R. Dimitrov, A. Mitchell, M. Stutzmann, J. Appl. Phys. 87 (1999) 334.

[9] V. Fiorentini, M. Methfessel, M. Scheffler, Phys. Rev. B 47 (1993) 13353.

[10] A. Rubio, J. L. Corkill, M. L. Cohen, E.L. Shirley, S. G. Louie, Phys. Rev. B 48 (1993) 11810.

[11] D. W. Jenkins, J. D. Dow, Phys. Rev. B 39 (1989) 3317.

[12] E. A. Albanesi, W. R. L. Lambrecht, B. Segall, Phys. Rev. B 48 (1993) 17841.

[13] G. D. Chen, M. Smith, J. Y. Lin, H. X. Jiang, Su-Huai Wei, M. Asif Khan, C. J. Sun, Appl. Phys. Lett. 68 (1996) 2784.

[14] W. Shan, I. J. Schmidt, X. H. Yang, S. J. Hwang, J. J. Song, Appl. Phys. Lett. 66 (1995) 985.

[15] H. Morkoc, *Nitride Semiconductors and Devices*, Springer Series in Materials Science, Springer, New York, 1999.

[16] F. Bernardini, V. Fiorentini, D. Vanderbilt, Phys. Rev. B 56 (1997) R10024.

[17] E. Berkowicz, D. Geshoni, G. Bahir, E. Lakin, D. Shilo, E. Zolotoyabko, A. Abare, S. DenBaars, L. Coldren, Phys. Rev. B 61 (2000) 10994.

[18] S. Chichibu, A. Shikanai, T. Deguchi, A. Setoguchi, R. Nakai, H. Nakanishi, K. Wada, S. DenBaars, T. Sota, S. Nakamura, Jpn. J. Appl. Phys. 39 (2000) 2417.

[19] A. Chakraborty, S. Keller, C. Meier, B.A. Haskell, P. Waltereit, S.P. DenBaars, S. Nakamura, J.S. Speck, U.K. Mishra, Appl. Phys. Lett. 86 (2005) 31901.

[20] T. Böttcher, Heteroepitaxy of group III nitrides for the application in laser diodes, dissertation, University of Bremen (2002).

[21] H. E. Bennet, J. O. Porteus, J. Opt. Soc. Am. 51 (1961) 123.

[22] K. Shiojima, J. Vac. Sci. Technol. B 18 (2000) 37.

[23] P. Visconti, D. Huang, M. A. Reshchikov, F. Yun, R. Cingolani, D. J. Smith, J. Jasinski, W. Swider, Z. Liliental-Weber, H. Morkoc, Mat. Sci. Eng. B 93 (2002) 229.

[24] D. A. Stocker, E. F. Schubert, J. M. Redwing, Appl. Phys. Lett. 73 (1998) 2654.

[25] B. Heying, X. H. Wu, S. Keller, Y. Li, D. Kapolnek, B. P. Keller, S. P. DenBaars, J. S. Speck, Appl. Phys. Lett. 68 (1996) 643.

[26] J. Matthews, A. Blakeslee, J. Cryst. Growth 32 (1974) 265.

[27] V. Kirchner, H. Heinke, D. Hommel, J. Z. Domagala, M. Leszczynski, Appl. Phys. Lett. 77 (2000) 1434.

[28] S. Nakamura, T. Mukai, M. Senoh, Appl. Phys. Lett. 64 (1994) 1687.

[29] S. Nakamura, M. Senoh, N. Iwasa, S. Nagahama, Jpn. J. Appl. Phys. 34 (1995) L797.

[30] S. Nakamura, M. Senoh, S. Nagahama, N. Iwasa, T. Yamada, T. Matsushita, H. Kiyoku, Y. Sugimoto, Jpn. J. Appl. Phys. 35 (1996) L74.

[31] K. Harafuji, Y. Hasegawa, A. Ishibashi, A. Tsujimura, I. Kidoguchi, Y. Ban, K. Ohnaka, Jpn. J. Appl. Phys. 39 (2000) 6180.

[32] H. Maruska, J. Tietjen, Appl. Phys. Lett. 15 (1969) 327.

[33] D. D. Koleske, M. E. Coltrin, A. A. Allerman, K. C. Cross, C. C. Mitchell, J. J. Figiel, Appl. Phys. Lett. 82 (2003) 1170.

[34] M. Lada, A. G. Cullis, P. J. Parbrook, J. Cryst. Growth 258 (2003) 89.

[35] X. H. Wu, P. Fini, E. J. Tarsa, B. Heying, S. Keller, U. K. Mishra, S. P. DenBaars, J. S. Speck, J. Cryst. Growth 189/190 (1998) 231.

[36] X. Wu, L. Brown, D. Kapolnek, S. Keller, B. Keller, S. DenBaars, J. Speck, J. Appl. Phys. 80 (1996) 3228.

[37] R. Chierchia, T. Böttcher, H. Heinke, S. Einfeldt, S. Figge, D. Hommel, J. Appl. Phys. 93 (2003) 8918.

[38] F. Degave, P. Ruterana, G. Nouet, J. H. Je, C. C. Kim, Mat. Sci. Eng. B B93 (2002) 177.

[39] P. Fini, X. Wu, E. Tarsa, Y. Golan, V. Srikant, S. Keller, S. DenBaars, J. Speck, Jpn. J. Appl. Phys. 37 (1998) 4460.

[40] S. J. Rosner, E. C. Carr, M. J. Ludowise, G. Girolami, H. I. Erikson, Appl. Phys. Lett. 70 (1997) 420.

[41] S. Nakamura, M. Senoh, S. Nagahama, N. Iwasa, T. Yamada, T. Matsushita, Y. Sugimoto, H. Kiyoku, Jpn. J. Appl. Phys. 36 (1997) L1059.

[42] O. Nam, M. D. Bremser, T. S. Zheleva, R. F. Davis, Appl. Phys. Lett. 71 (1997) 2638.

[43] P. Gibart, Rep. Prog. Phys. 67 (2004) 667.

[44] S. Haffouz, H. Lahreche, P. Vennegues, P. de Mierry, B. Beaumont, F. Omnes, P. Gibart, Appl. Phys. Lett. 73 (1998) 1278.

[45] R. Datta, M. J. Kappers, M. E. Vickers, J. S. Barnard, C. J. Humphreys, Superlattices and Microstructures 36 (2004) 393.

[46] P. Vennegues, B. Beaumont, V. Bousquet, M. Vaille, P. Gibart, J. Appl. Phys. 87 (2000) 4175.

[47] R. F. Davis, T. Gehrke, K. J. Linthicum, T. S. Zheleva, E. A. Preble, P. Rajagopal, C. A. Zorman, M. Mehregany, J. Cryst. Growth 225 (2001) 134.

[48] A. E. Romanov, P. Fini, J. S. Speck, J. Appl. Phys. 93 (2003) 106.

[49] A. E. Romanov, W. Pompe, G. E. Beltz, J. S. Speck, Appl. Phys. Lett. 69 (1996) 3342.

[50] J. S. Speck, M. A. Brewer, G. E. Beltz, A. E. Romanov, W. Pompe, J. Appl. Phys. 80 (1996) 3808.

[51] S. K. Mathis, A. E. Romanov, L. F. Chen, G. E. Beltz, W. Pompe, J. S. Speck, phys. stat. sol. (a) 179 (2000) 125.

[52] H. Klapper, Mater. Chem. Phys. 66 (2000) 101.

[53] S. Figge, T. Böttcher, S. Einfeldt, D. Hommel, J. Cryst. Growth 221 (2000) 262.

[54] X. H. Wu, D. Kapolnek, E. J. Tarsa, B. Heying, S. Keller, B. P. Keller, U. K. Mishra, S. P. DenBaars, J. S. Speck, Appl. Phys. Lett. 68 (1996) 1371.

[55] B. Heying, X. H. Wu, S. Keller, Y. Li, D. Kapolnek, B. P. Keller, S. P. DenBaars, J. S. Speck, Appl. Phys. Lett. 68 (1996) 643.

[56] T. Hashimoto, M. Yuri, M. Ishida, Y. Terakoshi, O. Imafuji, T. Sugino, K. Itoh, Jpn. J. Appl. Phys. 38 (1999) 6605.

[57] E. Frayssinet, B. Beaumont, J. P. Faurie, P. Gibart, Z. Makkai, B. Pecz, P. Lefebvre, P. Valvin, MRS Internet J. Nitride Semicon. Res. 7 (2002) 8.

[58] D. D. Koleske, A. E. Wickenden, R. L. Henry, W. J. DeSisto, R. J. Gorman, J. Appl. Phys. 84 (1998) 1998.

[59] H. Liu, J. G. Kim, M. H. Ludwig, R. M. Park, Appl. Phys. Lett. 71 (1997) 347.

[60] D. D. Koleske, M. E. Coltrin, K. C. Cross, C. C. Mitchell, A. A. Allerman, J. Cryst. Growth 273 (2004) 86.

[61] K. Lorenz, M. Gonsalves, W. Kim, V. Narayanan, S. Mahajan, Appl. Phys. Lett. 77 (2000) 3391.

[62] D. D. Koleske, A. E. Wickenden, R. L. Henry, J. C. Culbertson, M. E. Twigg, J. Cryst. Growth 223 (2001) 466.

[63] J. Chen, S. M. Zhang, B. S. Zhang, J. J. Zhu, G. Feng, X. M. Shen, Y. T. Wang, H. Yang, W. C. Zheng, J. Cryst. Growth 254 (2003) 348.

[64] S. Nakamura, Jap. J. Appl. Phys. 30 (1991) L1705.

[65] S. Kim, J. Oh, J. Kang, D. Kim, J. Won, J. Kim, H. Cho, J. Cryst. Growth 262 (2004) 7.

[66] B. Heying, X. H. Wu, S. Keller, Y. Li, D. Kapolnek, B. P. Keller, S. P. DenBaars, J. S. Speck, Appl. Phys. Lett. 68 (1996) 643.

[67] P. Fewster, *X-Ray Scattering from Semiconductors* (Imperial College Press, London 2000).

[68] T. C. Wen, W. I. Lee, J. K. Sheu, G. C. Chi, Solid-State Electronics 46 (2002) 555.

[69] C. F. Shih, M. Y. Keh, Y. N. Wang, N. C. Chen, C. Chang, P. H. Chang, K. S. Liu, J. Cryst. Growth 277 (2005) 44.

[70] S. Kamiyama, M. Iwaya, N. Hayashi, T. Takeuchi, H. Amano, I. Akasaki, S. Watanabe, Y. Kaneko, N. Yamada, J. Cryst. Growth 223 (2001) 83.

[71] H. Amano, I. Akasaki, Optical Materials 19 (2002) 219.

[72] H. Miyake, A. Motogaito, K. Hiramatsu, Jpn. J. Appl. Phys. 38 (1999) L1000.

[73] A. Usui, H. Sunakawa, A. Sakai, A. A. Yamaguchi, Jpn. J. Appl. Phys. 36 (1997) L899.

[74] T. Kawashima, K. Iida, Y. Miyake, A. Honshio, H. Kasugai, M. Imura, M. Iwaya, S. Kamiyama, H. Amano, I. Akasaki, J. Cryst Growth 272 (2004) 377.

[75] Y. Koide, N. Itoh, K. Itoh, N. Sawaki, I. Akasaki, Jpn. J. Appl. Phys. 27 (1988) 1156.

[76] A. E. Romanov, J. S. Speck, Appl. Phys. Lett. 83 (2003) 2569.